JRC Scientific and Technical Reports

A biology-based dynamic approach for the modelling of toxicity in cell assays: Part II: Models for cell population growth and toxicity

J. M. Zaldívar, M. Mennecozzi, P. Macko, R. Rodrigues, M. Bouhifd and J. Baraibar

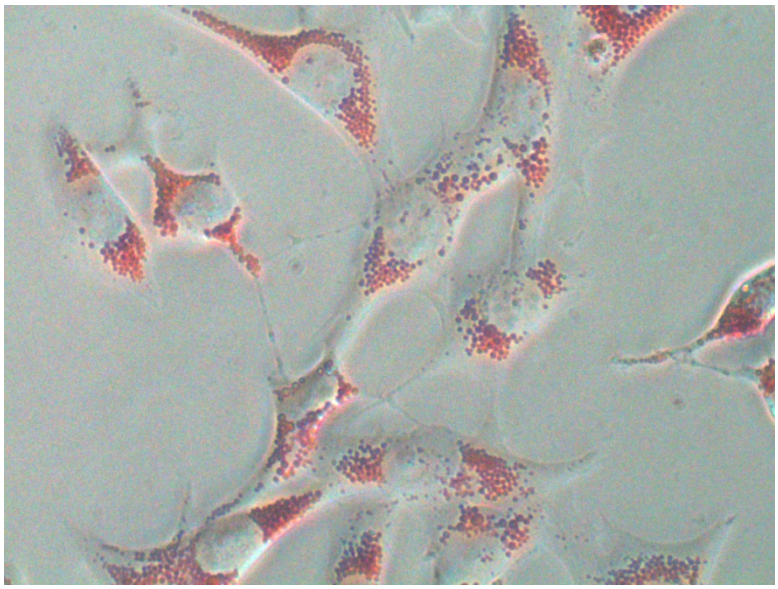

EUR 24374 EN - 2011

JRC EUROPEAN COMMISSION

ihcp Institute for Health and Consumer Protection

The mission of the JRC-IHCP is to protect the interests and health of the consumer in the framework of EU legislation on chemicals, food, and consumer products by providing scientific and technical support including risk-benefit assessment and analysis of traceability.

European Commission
Joint Research Centre
Institute for Health and Consumer Protection

Contact information
Address: Via E. Fermi 2749, TP 202, 21027 Ispra(VA), Italy
E-mail: jose.zaldivar-comenges@jrc.ec.europa.eu
Tel.: +39-0332-789202
Fax: +39-0332-789963

http://ihcp.jrc.ec.europa.eu/
http://www.jrc.ec.europa.eu/

Legal Notice
Neither the European Commission nor any person acting on behalf of the Commission is responsible for the use which might be made of this publication.

Europe Direct is a service to help you find answers to your questions about the European Union

Freephone number (*):

00 800 6 7 8 9 10 11

(*) Certain mobile telephone operators do not allow access to 00 800 numbers or these calls may be billed.

A great deal of additional information on the European Union is available on the Internet.
It can be accessed through the Europa server http://europa.eu/

JRC 63686

EUR 24374 EN
ISBN 978-92-79-19568-6
ISSN 1831-9424
doi:10.2788/61603

Luxembourg: Publications Office of the European Union

© European Union, 2011

Reproduction is authorised provided the source is acknowledged

Printed in Italy

EXECUTIVE SUMMARY

There is a need to extrapolate from *in vitro* concentrations to *in vivo* dose. To do this extrapolation it is necessary to be able to calculate free concentrations in both systems and then compare them. Concerning the *in vitro* side, in the first part of this work, we had developed and implemented, based on HTS (High Throughput Screening) laboratory data, a compound fate model using the partitioning approach. The developed fate model was able to predict the role of serum in toxicity assays as well as provide estimation on the partitioning of a certain compound between the headspace, plastic wall and the medium: attached to serum, free dissolved and attached to the cells. However, the partitioning approach assumes that the equilibrium is fast in comparison with the duration of the experiments, which could not be the case for the partitioning to the cells. For this reason, a DEB (Dynamic Energy Budget) stage-based toxicity model has been developed and experimentally verified in the second part of this work. In addition, the model allows using internal concentrations as another toxicity scale allowing a toxicodynamics' independent raking of the toxic potency of a chemical and the possibility of toxicity data reconciliation from several sources taking into account the inherent dynamics always present during cell-based assays. The results show that this approach opens a new way of analyzing this type of data sets and offers the possibility of extrapolating the values obtained to calculate *in vivo* human toxicology thresholds using a PBTK modelling approach.

CONTENTS

CONTENTS ii
1. INTRODUCTION 1
2. METHODS AND APPROACH 2
2.1. CELL ASSAYS GROWTH AND DIVISON MODEL 3
2.2. BIOCONCENTRATION AND BIOACCUMULATION IN CELLS 4
2.3. TOXICITY AND EFFECTS MODELS 7
2.4. ESTIMATION OF MODEL'S PARAMETERS AND CORRELATIONS 8
2.4.1. Experimental set-up characteristics 8
2.4.2. Concentration-response curves 9
2.4.3. Measuring cell population 12
2.4.4. Estimation of the chemical partitioning inside the cell 14
2.4.5. Estimation of cell permeability 15
2.5. OPTIMIZATION PROCEDURE FOR FITTING CONCENTRATION-RESPONSE CURVES 17
3. RESULTS AND DISCUSSION 17
3.1. STAGE-BASED 3T3 CELL GROWTH MODEL 17
3.2. TOXICITY ASSAYS 18
3.2.1. Estimation of the killing rate and the no-effect concentration 18
3.2.2. Global estimation of model's parameters 30
3.2.3. Simulation of the cell population experiments 33
3.3. IN VITRO –IN VIVO EXTRAPOLATION 34
3.4. PREDICTION OF 24 h ACUTE TOXICITY IC_{50}s 36
3.5. REPEAT DOSE SIMULATION 36
4. CONCLUSIONS 37
5. REFERENCES 39
APPENDIX A. FATE AND TRANSPORT: MASS BALANCE MODEL 42
APPENDIX B. NOTATION 48

1. INTRODUCTION

The need for animal replacement in toxicology testing calls for the development of an Integrated Testing Strategy (ITS) able to move from *in vitro* toxic concentrations to *in vivo* dose without the passage to animal testing and the application of the corresponding assessment factors. This implies the need to consider toxicodynamics as an important, if not essential, part in the risk assessment strategy (Pelkonen *et al*., 2011). The characterization of the concentration that produces the toxic effect it is necessary at two levels; first for the *in vitro* experiments since "nominal" concentrations does not represent the real concentration experienced by the cell and second in the extrapolation of the dose for human toxicity assessment since to assess the hazard of a chemical compound we need to know the real concentration experienced by the target organ. One possible way to solve both problems, and be able to compare the same concentrations from *in vitro* and *in vivo* experiments, is the use of biology/physiology-based toxicodynamic models at both levels. For *in vitro* experiments a model comprising the fate of a compound in the cell-based assay, i.e. its partitioning between plastic wall, serum proteins and lipids, as well as the dynamics within the cell combined with a toxic effect model and, if necessary, a cell growth model, constitute the basis for the calculation of the realistic conditions when direct concentration measurements are not possible. For the establishment of a safe *in vivo* human dose intake reverse dosimetry, based on a battery of *in vitro* test, using Physiological Based Toxicokinetics models -PBTK or PBPK-(Clewell *et al.* 2008) seems the most promising route to explore.

The first attempts to assess the applicability of this strategy for the safety evaluation of chemicals were based on the following elements (DeJongh *et al*., 1999; Gubbels-van Hal *et al*., 2005):

- *in vitro*/ QSAR data on ADME (Absorption, Distribution, Metabolism, Excretion) as input data to
- PBPK modelling (rat, human, etc.) for calculating target tissue concentration *in vivo* for the prediction of dose-response curves, NOEL (Not Observed Effect Level), LOEL (Lowest Observed Effect Level), etc.
- *in vitro* and *in vivo* studies to validate the approach.

The application of this approach to a reduced set of substances (10) to REACH requirements at production levels > 10 tonnes shown that it was possible to reduce by 38% the number of animals used, but further improvement was foreseen with the refinement of the procedure (Gubbels-van Hal *et al*., 2005).

Concerning *in vitro* tests the suggested refinements (Gubbels-van Hal *et al*., 2005) in the ITS included the need to estimate the partitioning and bioavailability of the chemical in the assay to improve the methodology used to relate *in vitro* toxic concentrations to *in vivo* target tissue concentrations.

In a more recent attempt, Rotroff *et al*. (2010) estimated the human oral equivalent dose necessary to produce equivalent concentration levels using a human PBTK model and *in vitro* toxicity AC_{50} values from ToxCast datasets (http://www.epa.gov/ncct/toxcast/chemicals.html) together with metabolic clearance and plasma protein binding experimental data. They found that two compounds over the 35 chemicals shown oral equivalent doses and estimated exposures which indicated the need to focus regulatory attention on these chemicals.

In the first part of this work (Zaldívar *et al*., 2010), we had developed and implemented, based on HTS (High Throughput Screening) laboratory data, a compound fate model using the partitioning approach. The developed fate model was able to predict the role of serum in toxicity assays as well as provide estimation on the partitioning of a certain compound between the headspace, plastic wall and the medium: attached to serum, free dissolved and attached to the cells. However, the partitioning approach assumes that the equilibrium is fast in comparison with the duration of the experiments which could not be the case for the partitioning to the cells. For this reason, a DEB (Dynamic Energy Budget) stage-based toxicity model (Kooijman, 2000) has been developed and experimentally verified in the second part of this work.

In addition, an aspect as important as the partitioning of the chemical in the cell assay is the dynamics of the cells during the experiment. The fundamental process is the growth of the cell population which will change the partitioning during the experiment and therefore the toxic effects experienced by the cells. In principle growth may be seen as a dilution process, but also affects the dynamics of the compound exchange between the cells as the medium. Furthermore, some cells are able to release proteins and lipids to the medium, e.g. albumin by HEPG2 cells that may also change the partitioning. The results of the model has been used to analyze the Neutral Red Uptake (NRU) cytotoxicity assay using the BALB/c 3T3 cells for several compounds This approach opens a new way of analyzing this type of data sets and it offers the possibility of extrapolating the values obtained to calculate *in vivo* human toxicology thresholds using reverse dosimetry in a PBTK modelling set-up.

2. METHODS AND APPROACH

Normally dose-response curves in *in vitro* experiments are represented using the total amount of substance added and not the dissolved (free) concentration which is the bioavailable fraction able to produce a toxic effect. Therefore, *in vitro* dose response curves (or their potency data e.g. EC_{50}, IC_{50} values) does not properly reflect the real toxic potency of a chemical since the compound will partition into the medium dissolved organic and particulate organic carbon (mainly serum and cells), and into the plastic walls as well as into the headspace (Gülden at al., 2001; Heringa et al., 2004; Kramer, 2010, amongst others). Another aspect that should be considered when volatile compounds are tested is the possibility of evaporation and cross contamination.

In addition, during the experiments cells growth and divide consuming nutrients, therefore the partitioning characteristic of the medium changes with time as well as the internal concentrations in the cells, complicating even further the comparison between different *in vitro* experiments and systems and therefore call for an integrated modelling approach able to quantify all this aspects and to "correct" the nominal concentrations as a function of the cell assay and the physico-chemical properties of the tested compounds. Therefore this integrated modelling approach must consist of:

- A fate and transport model
- A cell growth and division model
- A toxicodynamics model

The solution of the ordinary differential equations of the model should allow the calculation over time of the dissolved concentration of a chemical as well as the internal concentration in the cell assay. We are briefly going to illustrate the different models and how they are interrelated.

In this second work, we will develop and test the growth and toxicodynamics models coupled with the fate and transport model previously developed in Zaldívar *et al*. (2010).

2.1. CELL ASSAYS GROWTH AND DIVISION MODEL

The use of continuous ordinary differential equations ignores population structure by treating all individuals as identical. The existence of demographically important differences among individuals is obvious. Matrix population models (Caswell, 1989) integrate population dynamics and population structure and they are very useful when the life cycle is described in terms of size classes or age classes. There are fundamentally two types of approaches, the age classified model and the stage classified model. The first one assumes age-specific survival and fertility are sufficient to determine population dynamics. On the other hand, if the vital rates depend on body size, and growth is sufficiently plastic that individuals of the same age may differ appreciably in size, then age will provide little information about the fate of an individual (e.g. fish models, see Zaldívar and Campolongo, 2000). For the case of the 3T3 cell model, we have considered that the appropriate description corresponds to a four stage-based approach, each stage corresponding to one of the four cell cycle phases: G1, S, G2, M (Hartell and Weinert, 1989).

In the stage-based type of modelling the matrix $\boldsymbol{A}$, called Leslie matrix, which describes the transformation of a population from time t to time t+1,

$$\boldsymbol{n}_{t+1} = \boldsymbol{A}\, \boldsymbol{n}_t \qquad (1)$$

has the following structure:

$$\mathbf{A} = \begin{bmatrix} P_1 & 0 & ... & ... & F \\ G_1 & P_2 & 0 & ... & 0 \\ 0 & G_2 & P_3 & 0... & 0 \\ ... & ... & ... & ... & ... \\ 0 & 0 & 0... & G_{q-1} & P_q \end{bmatrix} \quad (2)$$

where $\boldsymbol{n}_t$ is a vector describing the population at each stage at time t, P_i is the probability of surviving and staying in stage i; G_i is the probability of surviving and growing into the next stage, and F is the fecundity rate per unit time (h), $i = 1,2,...,q$.

Both P_i and G_i are functions of the survival probability p_i and the growth probability γ_i (Caswell 1989):

$$P_i = p_i(1-\gamma_i) \quad (3)$$

$$G_i = p_i \cdot \gamma_i \quad (4)$$

where

$$p_i = \exp(-z_i) \quad (5)$$

and

$$\gamma_i = \frac{(1-p_i)p_i^{d_i-1}}{1-p_i^{d_i}} \quad (6)$$

where z_i is the hourly instantaneous mortality rate and d_i is the duration (h) within the i-th stage.

Incorporation of interaction between species at different stages can be easily done (Cushing, 1998; Zaldívar and Campolongo, 2000).

2.2. BIOCONCENTRATION AND BIOACCUMULATION IN CELLS

Simple mass balance models of a contaminant in an organism (Thomann, 1989 and Thomann et al., 1992) consider the organisms as a single compartment. A more complete model was developed, based on the Dynamic Energy Budget (DEB) approach, by Kooijman and van Haren (1990) and van Haren et al. (1994) that takes into account changes in lipid contents and size of the organisms. With this approach toxic effects introduced at population level can be extended to ecosystem level. The introduction of DEB models into matrix population models has been developed recently (Lopes et al., 2005; Klanjscek et al., 2006; Billoir et al., 2007). Following this approach, we have considered that once the chemical is taken up by the cell it partition instantaneously over three compartments: one aqueous fraction and two non-aqueous fractions: structural component (proteins) and the energy reserves (lipids). This approach is represented in Figure 1 following Kooijman and van Haren (1990).

In this case, the total number of moles of a compound in the organism can be divided as the sum of them in the different compartments:

$$n_{tot} = n_{aq} + n_P + n_L = (V_{aq} \cdot C_{aq} + V_P \cdot C_P + V_L \cdot C_L) \quad (7)$$

where the V_i's refer to the compartment volumes (l) and the C_i's refer to the compartments

concentrations (mol l^{-1}). Also, the total number of moles of a chemical can be expressed as:

$$n_{tot} = W \cdot C_b / MW \quad (8)$$

where W is the organisms weight (g), MW is the molecular weight of the chemical (g mol^{-1}) and C_b is the contaminant concentration in the cell ($g \cdot gww^{-1}$) .

The chemical is assumed to be in equilibrium between the different compartments with fixed values partition coefficients: $K_P=C_p/C_{aq}$ and $K_L=C_L/C_{aq}$.

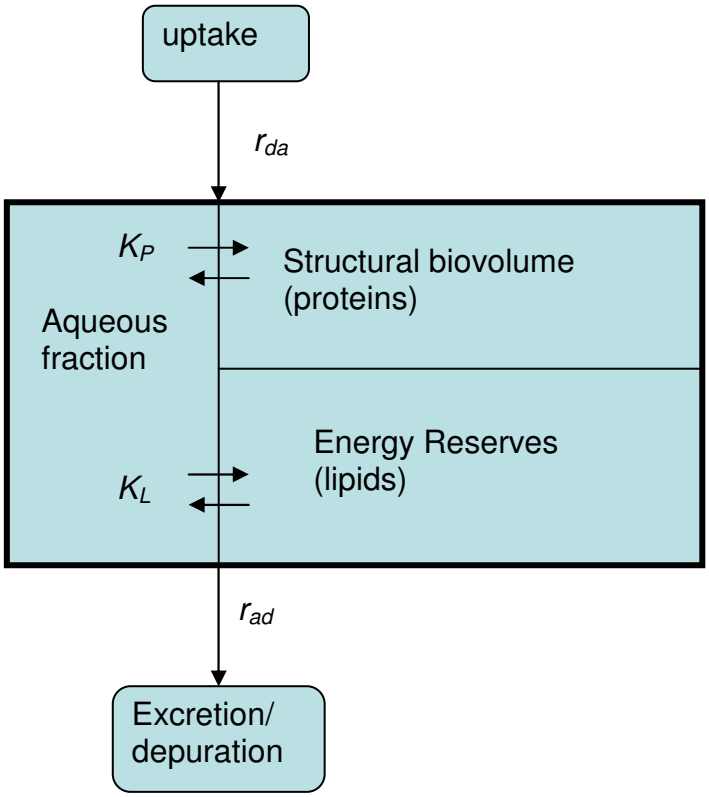

Figure 1. Schematic representation of the chemical partitioning in the cellular compartments.

The time evolution of this substance in the cell can be calculated by a simple mass balance, assuming that uptake and depuration rates, r_{da} and r_{ad} (l cm^{-2} s^{-1}), are proportional to the surface area of the cell (passive diffusion), and the transfer occurs through the aqueous compartment only (Kooijman, 2000), as:

$$\frac{dn_{tot}}{dt} = V^{2/3}(r_{da} \cdot C_{diss} - r_{ad} \cdot C_{aq}) \quad (9)$$

where C_{diss} and C_{aq} refer to the dissolved fraction concentration in the medium (mol l^{-1}) and in the aqueous compartment of the cell (mol l^{-1}), respectively. However, it is more convenient to express the mass balance as a function of the cell's concentration, C_b (g gww^{-1}). Therefore, applying the chain rule of derivation to Eq. (8), we have:

$$\frac{dn_{tot}}{dt} = \frac{1}{MW}\left(W\frac{dC_b}{dt} + C_b\frac{dW}{dt}\right) \quad (10)$$

and rearranging terms we obtain:

$$\frac{dC_b}{dt} = \frac{MW \cdot V^{2/3}}{W}(r_{da} \cdot C_{diss} - r_{ad} \cdot C_{aq}) - \frac{C_b}{W}\frac{dW}{dt} \quad (11)$$

In this case, the last term represents the dilution due to growth of the cell. This is a more realistic assumption that the linear-constant function assumed in the first bioaccumulation models (Thomman, 1989).

Since the concentration in the aqueous fraction, C_{aq}, is not a value that is measured, then we have to convert it in terms of C_b using the partitioning approach. The wet weight, W, can also be expressed as a function of the volumes of the different compartments times the density (ρ in g l^{-1}):

$$W = \rho \cdot V = \rho\left(V_{aq} + V_P + V_L\right) \quad (12)$$

For 3T3 ρ = 1195 g l^{-1} (Meisler, 1973). In addition, assuming that the mass proportion between proteins, lipids and aqueous fraction does not change appreciably in the cells during growth, the following relationships can be written:

$$V_P = W_P / \rho_P \quad (13)$$

$$V_L = W_L / \rho_L \quad (14)$$

$$V_{aq} = W_{aq} / \rho_{aq} \quad (15)$$

where W_P , W_L and W_{aq} are the masses of proteins, lipids and aqueous compartments in the cells and ρ_P, ρ_L and ρ_{aq} their densities, i.e, 1350, 900 and 1000 gl^{-1}, respectively.

To find the correlation between C_{aq} and C_b, we have to combine n_{tot} in Eqs. (7)-(8), the partition coefficients, and Eqs, (13)-(15), then we have:

$$C_{aq} = \frac{C_b}{MW\left(\frac{f_{aq}}{\rho_{aq}} + \frac{f_L}{\rho_L}K_L + \frac{f_P}{\rho_P}K_P\right)} \quad (16)$$

where the f_i refer to the mass fractions of each compartment (aqueous, lipid, proteins) in the cell. For 3T3 we have: f_{aq}=0.244, f_L=0.142; f_P= 0.614 (Meisler, 1973).

Replacing this equation into Eq. (11) and rearranging, we obtain a similar equation to the one proposed by Thomann (1989) and Thomann *et al*. (1992):

$$\frac{dC_b}{dt} = \left(\frac{MW \cdot V^{2/3}}{W} r_{da}\right) C_{diss} - \left(\frac{V^{2/3}}{W\left(\frac{f_{aq}}{\rho_{aq}} + \frac{f_L}{\rho_L}K_L + \frac{f_P}{\rho_P}K_P\right)} r_{ad}\right) C_b - \left(\frac{1}{W}\frac{dW}{dt}\right) C_b \quad (17)$$

However in this case uptake and depuration rates are not constant, but depend on the status of the cell and take into account the differences in growth.

The variation of the wet weight, W, as a function of time can be obtained, assuming constant

composition and hence density, as:

$$\frac{dW}{dt} = \rho \frac{dV}{dt} \tag{18}$$

If we consider spherical shape, $V = \frac{4}{3}\pi r^3$, and von Bertalanffy's growth curve

$$r(t) = r_\infty - (r_\infty - r_0)e^{-\alpha_G \cdot t} \tag{19}$$

where r_0 and r_∞ refer to the initial and final cell radius and α_G is the von Bertalanffy's growth rate. Then we have:

$$\frac{dV}{dt} = 4 \cdot \pi \left[r_\infty - (r_\infty - r_0)\exp(-\alpha_G \cdot t) \right]^2 (r_\infty - r_0) \cdot \alpha_G \cdot \exp(-\alpha_G \cdot t) \tag{20}$$

For 3T3: r_∞=8.3057·10^{-6} m , r_0=6.592·10^{-6} m, and α_G=1.268·10^{-4}.

However, the introduction of this term considers only a single cell developing during the simulation. To consider the whole population of the cells, instead of a single cell, we will take average values for the weight, its derivative, and the surface depending on the four stages: G1, S, G2, M.

The model in Eq. (17) has several parameters that need to be evaluated. The uptake and depuration rates, r_{da} and r_{ad}, and the partition coefficients, K_L and K_P, depend on the compound; whereas the remain parameters depend on the type of cell we are modelling.

2.3. TOXICITY AND EFFECTS MODELS

The direct effects of a chemical concentration, C, on survival may be expressed, using Eq. (5), by the addition of a term which can be written as:

$$z_i = \begin{cases} z_i + k_t(C_b - NEC) & \text{if } C > NEC \text{ and } \tau > \tau_0 \\ z_i \end{cases} \tag{21}$$

where C_b is the internal concentration of the toxicant in the cell, k_t is the killing rate and NEC is the no effect concentration term (Lopes et al., 2005; Billoir et al., 2007). This equation will modify the terms P_i and G_i ,i.e., Eqs. (3)-(4), in the stage-based Leslie matrix Eq. (2). In principle, it is possible to introduce a different expression for each cell stage. However, for simplicity reasons and due to the fact that the data to validate the model does not allow to distinguish this aspect, we have considered global k_t and NEC values. Furthermore, even though in this work we have only considered mortality effects, other effects could also be treated using a similar approach by introducing different expressions in the toxicity effects model. This was already proposed and developed by Kooijman and Bedaux (1996) who considered effects in reproduction for *Daphnia magna* and other organisms. In the case of cell-based assays a fecundity rate expression that modifies F as a function of chemical concentration could also be developed, i.e.

$$F = \begin{cases} F - k_F(C_b - NEC_F) & \text{if } C > NEC_F \text{ and } \tau > \tau_0 \\ F \end{cases} \tag{22}$$

2.4. ESTIMATION OF MODEL'S PARAMETERS AND CORRELATIONS

2.4.1. Experimental set-up characteristics

The experimental procedure for the 3T3 BALB/c Neutral Red Uptake (NRU) cytotoxicity assay was developed for the NICEATM/ECVAM validations study requirements (ICCVAM, 2006a, b), whereas issues concerning the automation and the implementation of the assay using the Pilot Test Platform (PTP) of the IHCP automated test facility may be found in Bouhifd et al. (2005) and Bouhifd and Whelan (2006).

The results of the testing for the validation study have been reported in ICCVAM (2006a) whereas the results obtained by testing 28 chemicals at the High Throughput Screening (HTS) platform are described in Norlén et al. (2007).

The configuration of the 96-well test plate is shown in Fig.2. The dimensions of each well are:

- Top internal radius: $3.425 \cdot 10^{-3}$ m.
- Bottom internal diameter: $3.175 \cdot 10^{-3}$ m.
- Depth: $10.76 \cdot 10^{-3}$ m.
- Bottom area $3.16 \cdot 10^{-5}$ m^2

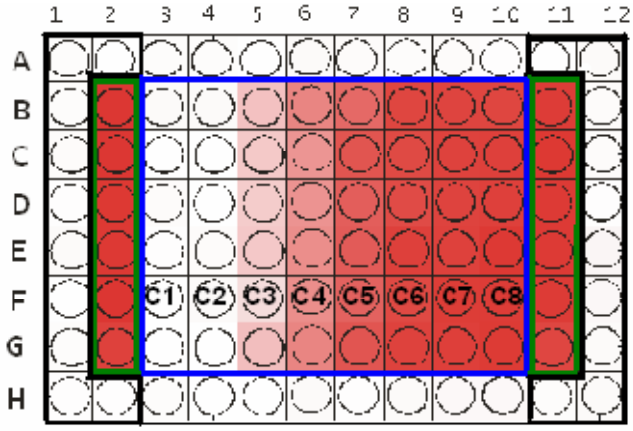

Figure 2. Configuration of the 96-well test plate. Blue: cells with dosing solutions of test chemical, six replicates for each dose and eight concentrations, C1 is the highest and C8 is the lowest concentration; green: Black: only medium, blank experiments; green: Vehicle Controls (VC), contain cells in medium and no test compound (the VCs are considered to have 100% viability).

With these dimensions and assuming the experiments contained 100 µL, i.e. $V_M = 10^{-7}$ m^3, we can obtain:

- Total well volume (assuming a truncated cone):

$$V_W = \frac{1}{3}\pi\left(r^2 + r \cdot R + R^2\right)h = 3.683 \cdot 10^{-7} \text{ m}^3.$$

- Headspace volume (m^3): $V_H = 2.683 \cdot 10^{-7}$ m^3.

- Surface of the well in contact with the medium, $S_M = \pi(r + r_m)g + S_{bottom}$, where r_m is the radius of the occupied volume and g is the slant height. $S_M = 9.392 \cdot 10^{-5}$ m^2.

- Surface of the cell-based assay medium, $A_S = \pi \cdot r_m^2 = 3.312 \cdot 10^{-5}$ m^2.

Assuming a 5% (v/v) serum in the medium, then $[S]_0 = 2.34\ 10^{-2}$ mol protein m^{-3}.

2.4.2. Concentration-response curves

In this work we have used dose-response curves obtained at the HTS laboratory using the 3T3 BALB/c Neutral Red Uptake (NRU) cytotoxicity assay for the twenty compounds described in Table 1. These compounds have been used in several international exercises, eg., the NICEATM/ECVAM validation study and were studied previously in the laboratory (Norlén et al., 2007).

Table 1. List of selected compounds.

Compound	CAS number	Compound	CAS number
Acetaminophen	103-90-2	Amiodarone hydrochloride	19774-82-4
Verapamil hydrochloride	152-11-4	Caffeine	58-08-2
Acetylsalicylic acid	50-78-2	Carbamazepine	298-46-4
Maprotiline	10262-69-8	Colchicine	64-86-8
Cycloheximide	66-81-9	Acrylamide	79-06-1
Sodium lauryl sulfate	151-21-3	Diphenhydramine	58-73-1
tert-Butyl hydroperoxide	75-91-2	Pentachlorophenol	87-86-5
Valproic acid	99-66-1	Disopyramide	3737-09-5
Rifampin	13292-46-1	Chloroquine diphosphate	50-63-5
Thioridazine hydrochloride	130-61-0	Tetracycline hydrochloride	64-75-5

The physico-chemical properties and parameters that depend on the compound needed to run the model are described in Table 2. *MW*, log K_{ow} and *H* were obtained from EPI suite v4.0 (experimental values were preferred over predictions), the molecular volume at the boiling point -v_b- was calculated using the group method from Schotte (1992) and the contribution to the atomic diffusion volumes, Σv_B, for use in estimating *D* by the method of Fuller et al. (1966) were obtained by applying the values from Table A1 in the appendix to the selected compounds.

Figures 3 and 4 show the fitted concentration-response curves for the twenty selected chemicals, whereas in Table 3 the obtained IC50 values are compared with those provided by Clothier et al. (2008). Concentration response curves were fitted using the biphasic equations from Beckon et al. (2008):

$$y = \left(\frac{1}{1 + (\varepsilon_{up} / x)^{\beta_{up}}} \right) \left(\frac{1}{1 + (\varepsilon_{dn} / x)^{\beta_{dn}}} \right) \tag{23}$$

with $\beta_{up}>0$ and $\beta_{dn}<0$. Following Beckon et al. (2008) the β-values represent the steepness, whereas ε–values represent the dose at the mid-point of the rising and of the falling respectively. This approach was introduced by Beckon et al. (2008) to consider biphasic relationships in dose-response curves and

it can be extended to consider more than one positive and negative effect.

Table 2. Physico-chemical properties/parameters used in the model.

Compound	MW (g mol^{-1})	log K_{ow}	H (Pa m^3 mol^{-1})	V_b (cm^3 mol^{-1})	$\sum v_B$
Acetaminophen	151.17	0.46	$6.51 \cdot 10^{-8}$	159.98	146.27
Verapamil hydrochloride	491.08	3.45	$1.41 \cdot 10^{-9}$	966.03	535.12
Acetylsalicylic acid	180.16	1.19	$1.32 \cdot 10^{-4}$	178.06	166.06
Maprotiline	277.41	4.52	$8.08 \cdot 10^{-3}$	347.31	300.43
Cycloheximide	281.35	0.55	$3.57 \cdot 10^{-10}$	363.44	280.25
Sodium lauryl sulfate	288.38	1.60	$1.12 \cdot 10^{-10}$	359.59	286.42
tert-Butyl hydroperoxide	90.12	0.94	1.62	112.66	96.76
Valproic acid	144.22	2.75	$3.04 \cdot 10^{-1}$	194.78	174.64
Rifampin	822.96	4.24	$2.75 \cdot 10^{-37}$	850.96	811.86
Thioridazine hydrochloride	407.04	4.93	$9.56 \cdot 10^{-14}$	375.85	384.04
Amiodarone hydrochloride	645.32	7.57	$1.82 \cdot 10^{-7}$	523.10	447.45
Caffeine	194.19	-0.07	$3.63 \cdot 10^{-6}$	206.06	133.74
Carbamazepine	236.28	2.45	$1.10 \cdot 10^{-5}$	234.37	227.52
Colchicine	399.45	1.30	$1.82 \cdot 10^{-12}$	395.84	390.47
Acrylamide	71.08	-0.67	$5.98 \cdot 10^{-4}$	80.92	70.57
Diphenhydramine	255.36	3.27	$5.44 \cdot 10^{-4}$	298.91	292.85
Pentachlorophenol	266.34	5.12	$1.27 \cdot 10^{-2}$	192.27	183.73
Disopyramide	339.48	2.58	$2.62 \cdot 10^{-11}$	420.11	380.38
Chloroquine diphosphate	319.88	4.63	$1.09 \cdot 10^{-7}$	376.82	394.68
Tetracycline hydrochloride	482.92	-3.70	$1.27 \cdot 10^{-26}$	457.57	406.42

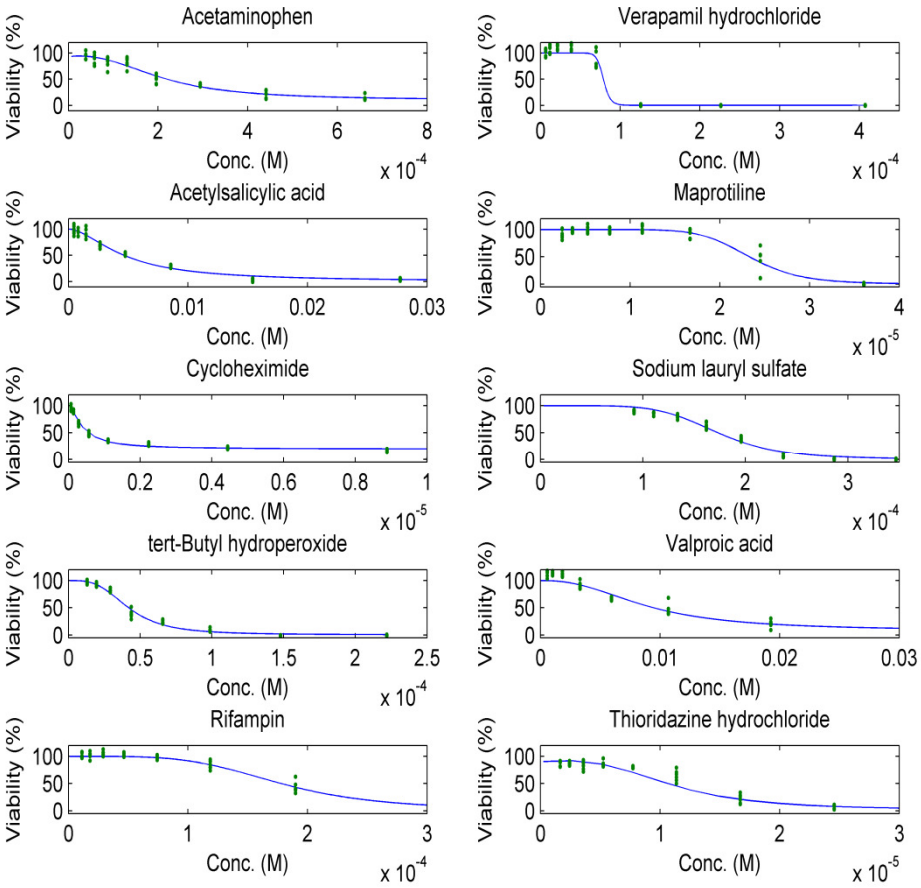

Figure 3. Concentration-response curves (experimental and fitted data) for the first set of selected chemicals.

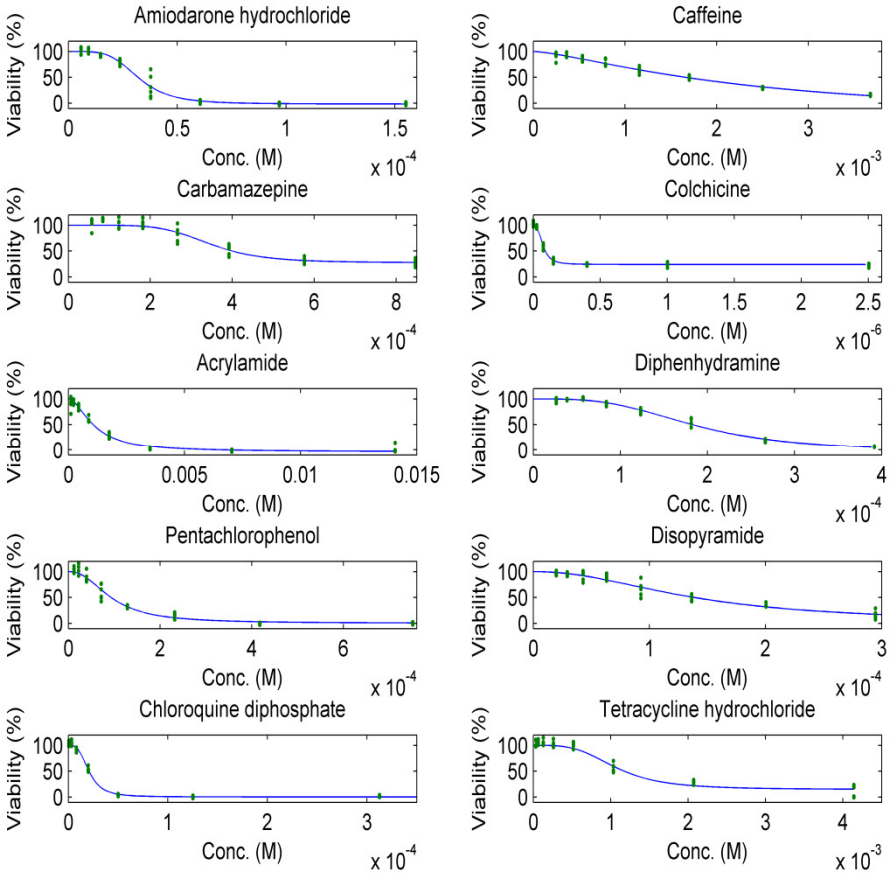

Figure 4. Concentration-response curves (experimental and fitted data) for the second set of selected chemicals.

Table 3. Calculated IC_{50} values compared with Clothier et al. (2008) and observed LD_{50} for the selected chemicals.

Compound	**IC_{50} (M)**	**IC_{50} (M) ± sd** Clothier et al. (2008)	**Observed LD_{50} (mg kg^{-1})**
Acetaminophen	$2.19 \cdot 10^{-4}$	$(3.32 \pm 1.20) \cdot 10^{-4}$	2052±187
Verapamil hydrochloride	$7.89 \cdot 10^{-5}$	$(7.25 \pm 1.59) \cdot 10^{-5}$	109
Acetylsalicylic acid	$4.66 \cdot 10^{-3}$	$(4.32 \pm 2.38) \cdot 10^{-4}$	818±660
Maprotiline	$2.33 \cdot 10^{-5}$	$(1.97 \pm 0.44) \cdot 10^{-5}$	700
Cycloheximide	$6.04 \cdot 10^{-7}$	$(1.04 \pm 1.24) \cdot 10^{-6}$	1.6±0.6
Sodium lauryl sulfate	$1.73 \cdot 10^{-4}$	$(1.61 \pm 0.28) \cdot 10^{-4}$	1254
tert-Butyl hydroperoxide	$4.20 \cdot 10^{-5}$	$(6.11 \pm 8.34) \cdot 10^{-5}$	388
Valproic acid	$9.48 \cdot 10^{-3}$	$5.78 \cdot 10^{-3}$	1471
Rifampin	$1.78 \cdot 10^{-4}$	$(1.01 \pm 1.05) \cdot 10^{-4}$	1272
Thioridazine hydrochloride	$1.07 \cdot 10^{-5}$	$(6.51 \pm 4.31) \cdot 10^{-5}$	1038
Amiodarone hydrochloride	$3.2 \cdot 10^{-5}$	$(2.63 \pm 1.05) \cdot 10^{-5}$	3000
Caffeine	$1.66 \cdot 10^{-3}$	$(8.31 \pm 2.55) \cdot 10^{-4}$	229±64
Carbamazepine	$4.06 \cdot 10^{-4}$	$(4.61 \pm 1.86) \cdot 10^{-4}$	2251±514
Colchicine	$9.15 \cdot 10^{-8}$	$(1.21 \pm 1.15) \cdot 10^{-7}$	11
Acrylamide	$1.11 \cdot 10^{-3}$	-	121±66
Diphenhydramine	$1.83 \cdot 10^{-4}$	-	380
Pentachlorophenol	$9.3 \cdot 10^{-5}$	$(1.91 \pm 3.54) \cdot 10^{-4}$	45±31
Disopyramide	$1.39 \cdot 10^{-4}$	$(2.70 \pm 2.52) \cdot 10^{-3}$	333
Chloroquine diphosphate	$2.08 \cdot 10^{-5}$	$(2.30 \pm 0.57) \cdot 10^{-5}$	500
Tetracycline hydrochloride	$1.18 \cdot 10^{-3}$	$(8.31 \pm 3.04) \cdot 10^{-4}$	6442

To account for degradation during the experiment, the estimated half-lives using the Level III fugacity multimedia model provided by EPI suite v4.0 (Mackay, 2001) were chosen and a degradation constant was calculated for water and air as described in the Appendix. The values are summarized in Table 4. In principle for the more biodegradable compounds in water, a 10% concentration decrease in 48 hours was obtained, whereas for the persistent compounds less than 1% concentration decrease will occur. In air, degradation is normally fast, but their amount depends on the volatility of the chemical. These values are only a crude approximation and do not take into account cell metabolism, but at least they give an indication on the chemical stability of the compound. Due to the absence of experimental concentration measurements during these experiments, the model optimization tried to improve this estimation in a second step as a function of the experimental concentration-response curves (see Results section).

Table 3. Degradation constants based on EPI estimated half-lives in water and in air.

Compound	k_{deg} (s^{-1})	$k_{\deg}^{air}$ (s^{-1})
Acetaminophen	$0.535 \cdot 10^{-6}$	$1.33 \cdot 10^{-5}$
Verapamil hydrochloride	$0.045 \cdot 10^{-6}$	$9.00 \cdot 10^{-5}$
Acetylsalicylic acid	$0.535 \cdot 10^{-6}$	$9.82 \cdot 10^{-7}$
Maprotiline	$0.214 \cdot 10^{-6}$	$7.05 \cdot 10^{-5}$
Cycloheximide	$0.214 \cdot 10^{-6}$	$4.91 \cdot 10^{-5}$
Sodium lauryl sulfate	$0.535 \cdot 10^{-6}$	$1.11 \cdot 10^{-5}$
tert-Butyl hydroperoxide	$0.535 \cdot 10^{-6}$	$2.25 \cdot 10^{-6}$
Valproic acid	$0.535 \cdot 10^{-6}$	$6.13 \cdot 10^{-6}$
Rifampin	$0.045 \cdot 10^{-6}$	$6.59 \cdot 10^{-4}$
Thioridazine hydrochloride	$0.134 \cdot 10^{-6}$	$1.93 \cdot 10^{-4}$
Amiodarone hydrochloride	$0.045 \cdot 10^{-6}$	$1.24 \cdot 10^{-4}$
Caffeine	$0.535 \cdot 10^{-6}$	$1.46 \cdot 10^{-5}$
Carbamazepine	$0.214 \cdot 10^{-6}$	$2.37 \cdot 10^{-4}$
Colchicine	$0.134 \cdot 10^{-6}$	$6.98 \cdot 10^{-4}$
Acrylamide	$0.535 \cdot 10^{-6}$	$9.63 \cdot 10^{-6}$
Diphenhydramine	$0.214 \cdot 10^{-6}$	$9.53 \cdot 10^{-5}$
Pentachlorophenol	$0.045 \cdot 10^{-6}$	$4.13 \cdot 10^{-7}$
Disopyramide	$0.045 \cdot 10^{-6}$	$9.39 \cdot 10^{-5}$
Chloroquine phosphate	$0.134 \cdot 10^{-6}$	$1.13 \cdot 10^{-4}$
Tetracycline hydrochloride	$0.134 \cdot 10^{-6}$	$1.54 \cdot 10^{-4}$

2.4.3. Measuring cell population

The Neutral Red Uptake (NRU) cytotoxicity assay is a validated method to measure the 3T3 cell population in wells relative to the negative control well. However, as it is a destructive assay it does not allow time-lapse monitoring of cell population growth over time. Therefore, we applied a non-invasive bright field imaging microscopy that made it possible to observe cell population, count their number, and track their divisions, detachments and apoptosis. The mouse BALB/c 3T3 cells were cultured in Dulbeco's Modified Eagle's Medium (DMEM) (Sigma, D 5796) supplemented with 10%

NCS. The cells were passaged at least three times in 75 cm^2 culture flasks (Corning 430641) before being seeded in 16 chamber slides (Invitrogen C-37000) at a density of approximately 2000 cells per well. Immediately after seeding the cell populations started to be monitored by the bright field imaging microscopy on an inverted motorised microscope Olympus IX81. The cell populations were monitored over 4 days recording one picture per well every 10 minutes. This process was fully automated and no intervention of an operator was needed. During microscopy analysis, optimal cell growth conditions were maintained by using a stage humidified incubator that kept the temperature constant at 37°C and the partial CO_2 pressure at 5%. After two days of incubation the culture medium was washed out and the tested chemicals dissolved in the culture medium (Verapamil: $1.22 \cdot 10^{-4}$M, Acetaminophen: $3.31 \cdot 10^{-4}$M and $6.62 \cdot 10^{-4}$M) were added to the wells. In two wells, which were used as negative control, the culture medium was changed for fresh one. At the beginning of the experiment the typical number of cells in the field of view of the microscope was in the range of 120-160. After 4 days, the number of cells in the non treated negative control wells was almost doubled, while in the treated wells it was progressively decaying over time. During picture analysis, only the cells that were well attached to the surface were taken into account. Results of the five populations are presented in fig. 5.

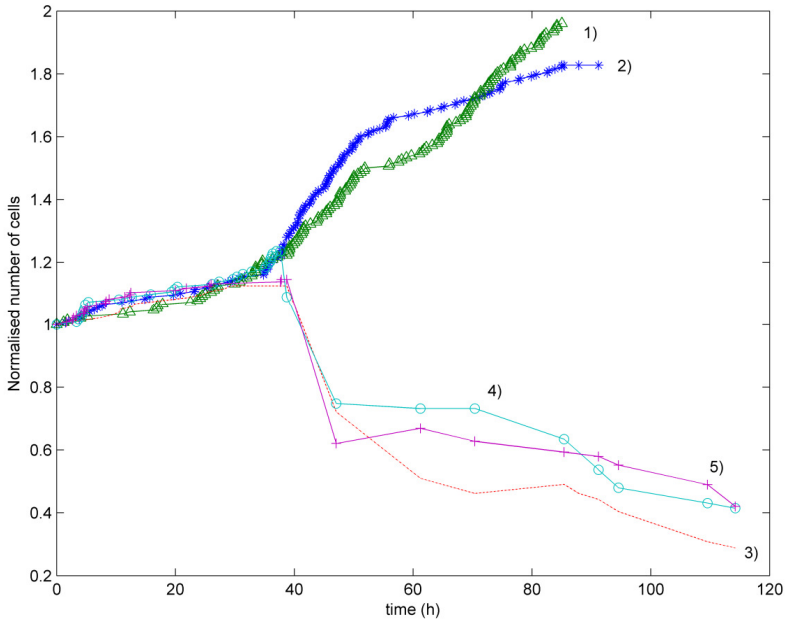

Figure 5. Curves for the five population experiments: 1) and 2) controls, 3) Verapamil $1.22 \cdot 10^{-4}$M, 4) Acetaminophen $3.31 \cdot 10^{-4}$M and 5) Acetaminophen $6.62 \cdot 10^{-4}$M added after 38.7 hours.

2.4.4. Estimation of the chemical partitioning inside the cell

A general approach to describe the distribution of the organic compound is by means of the partition coefficients K_i^c, defined as the relationships between the concentration in a particular component - for the cell proteins and lipids- and in the aqueous component. In this case we need to calculate K_P^c and

K_L^c. Several of these correlations have been found in literature and all of them assume that the compound has a linear sorption isotherm which is normally a good approximation at low concentrations, i.e. there is no saturation.

- Protein partitioning (K_P^c):

The protein partitioning coefficient can be expressed as:

$$K_P^c = \frac{C_P / [P]_c}{C_{aq}} \tag{24}$$

where $[P]_c$ is the concentration of proteins in the cell and the partition coefficient K_P^c is expressed in $m^3 \cdot mol^{-1}$. Therefore K_p in Eq. (16) is equal to: $K_P = K_P^c \cdot [P]_c$. For 3T3 we will assume a constant value, $[P]_c$ = 11.096 mol protein m^{-3} (Meisler, 1973).

In a compilation of blood protein (albumin) data DeBruyn and Gobas (2007) for different tissues found that the sorptive capacity of protein in solid animal tissues was higher than K_{ow} for low log K_{ow} chemicals (-1.3≤ log K_{ow} ≤1.09) with a value around 1.31(±0.62) (ml g^{-1} albumin). For more lipophobic chemicals (1.09 < log $K_{ow} \leq 4.6$) the logarithm of the partition constant increased with log K_{ow} following: 0.57 log K_{ow} +0.69, whereas at higher K_{ow} approached the lipid equivalence value of 0.05, i.e. log K_{ow}-1.3. Therefore, it is possible to write:

$$valp = \begin{cases} 1.31 \ \text{ if } \log K_{ow} < 1.09 \\ 0.57 \cdot \log K_{ow} + 0.69 \ \text{ if } 1.09 \geq \log K_{ow} \leq 4.6 \\ \log K_{ow} - 1.3 \ \text{ if } \log K_{ow} > 4.6 \end{cases} \tag{25}$$

and then,

$$K_P^c = 10^{(valp - 1.178)} \tag{26}$$

where 1.178 is a factor to convert ml g^{-1} albumin to m^3 mol^{-1} albumin. A MW = 66400 g mol^{-1} has been used for albumin.

- Lipid partitioning (K_L^c):

The partition coefficient of a chemical with cells lipids, K_L^c, could be written as:

$$K_L^c = \frac{C_L^c / [L]_c}{C_{aq}} \tag{27}$$

where $[L]_c$ is the concentration of lipids in the cell (kg m^{-3}). Therefore K_L in Eq. (16) is equal to: $K_L = K_L^c \cdot [L]_c$. For 3T3 cells, $[L]_c$= 170.4 kg m^{-3} (Meisler, 1973).

Jonker and van der Heijden (2007) found for PAHs a linear correlation between the lipid-water partition coefficient and the octanol-water partition coefficient as:

$$\log K_L^c = 1.25(\pm 0.06)\log K_{ow} - 3.70(\pm 0.37) \quad (28)$$

This correlation was used by Kramer (2010) to calculate the partitioning of PAHs in medium lipids. Similar correlations have been found by other authors for different families of substances, but in this work, we assume that this correlation holds for all the compounds.

Table 4. Estimated protein and lipid partition constants.

Compound	K_P^c (m^3 mol^{-1})	K_L^c (m^3 kg^{-1} lipid)
Acetaminophen	1.36	$7.50 \cdot 10^{-4}$
Verapamil hydrochloride	30.10	4.10
Acetylsalicylic acid	1.55	$6.10 \cdot 10^{-3}$
Maprotiline	122.57	89.13
Cycloheximide	1.36	$9.72 \cdot 10^{-4}$
Sodium lauryl sulfate	2.65	$2.0 \cdot 10^{-2}$
tert-Butyl hydroperoxide	1.36	$3.0 \cdot 10^{-3}$
Valproic acid	12.01	0.55
Rifampin	84.88	39.81
Thioridazine hydrochloride	283.14	290.07
Amiodarone hydrochloride	$1.236 \cdot 10^{5}$	$5.788 \cdot 10^{5}$
Caffeine	1.36	$1.63 \cdot 10^{-4}$
Carbamazepine	8.10	0.23
Colchicine	1.79	0.0084
Acrylamide	1.36	$2.90 \cdot 10^{-5}$
Diphenhydramine	23.76	2.44
Pentachlorophenol	438.53	501.19
Disopyramide	9.61	0.34
Chloroquine phosphate	141.91	122.32
Tetracycline hydrochloride	1.36	$4.73 \cdot 10^{-9}$

2.4.5. Estimation of cell permeability

Assuming passive diffusion as the only transport mechanism, it is possible to write (Del Vento and Dachs, 2002) that the uptake constant, k_{upt} (l g^{-1} d^{-1}), is given by:

$$k_{upt} = p \cdot S_p \quad (29)$$

where p (m d^{-1}) is the cell permeability and S_p is the specific surface of cells (m^2 Kg^{-1}), $S_p = V^{2/3}/W$.

There are several correlations to predict p as a function of physico-chemical properties of the molecule. In this work, we have used the experimental data obtained using caco-2 cells by Yazdanian et al. (1998) to fit an expression proposed in USEPA (1992) as a function of the octanol-water partition coefficient (K_{ow}) and the molecular weight (MW). The following correlation has been obtained:

$$\log p = -1.1711 + 0.98\log K_{ow} - 0.0011MW \quad (30)$$

where p is given in cm h^{-1}; to convert it to m d^{-1} then:

$$p = 0.24 \cdot 10^{(-1.1711 + 0.98\log K_{ow} - 0.0011MW)} \quad (31)$$

On the other hand, combining Eq. (29) and the first term in Eq. (17) it is possible to obtain the relationship between cell permeability and uptake rate:

$$k_{upt} = \frac{V^{2/3}}{W} r_{da} \tag{32}$$

Combining Eq. (29) with Eq. (31) r_{da} can be estimated as:

$$r_{da} = 10p \tag{33}$$

where 10 is a factor to convert m d^{-1} to $l \cdot cm^{-2}$ d^{-1}.

In a similar way the depuration constant, k_{dep} (d^{-1}) can be obtained as (Del Vento and Dachs, 2002):

$$k_{dep} = \frac{p \cdot S_p}{BCF} \tag{34}$$

where *BCF* is the Bioconcentration Factor (l g^{-1}) defined as the ratio of concentrations of the chemical in the cell and in water - freely dissolved - at equilibrium. In addition, considering Eqs. (29) and (34) it is possible to observe that the relationship between uptake and depuration constants depends only on the bioconcentration factor and by comparing Eq. (34) and the second rhs term in Eq. (17) we can observe that the uptake and depuration rates are equivalent, $r_{da}=r_{ad}$. Furthermore in our case the bioconcentration factor can be defined as:

$$BCF = \left(\frac{f_{aq}}{\rho_{aq}} + \frac{f_L}{\rho_L} K_L + \frac{f_P}{\rho_P} K_P \right) \tag{35}$$

Table 5 summarises the estimated values for r_{da}. These values have been used as initial parameters in the optimization procedure to fit experimental concentration-response curves, see Section 2.6.

Table 5. Estimated exchange rates constants of uptake and depuration between the cell and the medium and bioconcentration factors for 3T3.

Compound	r_{da} ($l \cdot cm^{-2}$ s^{-1})	***BCF*** ($l\ g^{-1}$)
Acetaminophen	$3.61 \cdot 10^{-6}$	0.071
Verapamil hydrochloride	$1.30 \cdot 10^{-3}$	0.2623
Acetylsalicylic acid	$1.74 \cdot 10^{-5}$	0.0082
Maprotiline	$2.49 \cdot 10^{-2}$	3.0150
Cycloheximide	$3.18 \cdot 10^{-6}$	0.0071
Sodium lauryl sulfate	$3.34 \cdot 10^{-5}$	0.0142
tert-Butyl hydroperoxide	$1.24 \cdot 10^{-5}$	0.0072
Valproic acid	$6.44 \cdot 10^{-4}$	0.0755
Rifampin	$3.30 \cdot 10^{-3}$	1.4989
Thioridazine hydrochloride	$4.53 \cdot 10^{-2}$	9.2277
Amiodarone hydrochloride	9.58	$1.6184 \cdot 10^{4}$
Caffeine	$9.78 \cdot 10^{-7}$	0.0071
Carbamazepine	$2.59 \cdot 10^{-4}$	0.0473
Colchicine	$1.28 \cdot 10^{-5}$	0.0095
Acrylamide	$3.45 \cdot 10^{-7}$	0.0071
Diphenhydramine	$1.60 \cdot 10^{-3}$	0.1858
Pentachlorophenol	$9.94 \cdot 10^{-2}$	15.6879
Disopyramide	$2.68 \cdot 10^{-4}$	0.0577
Chloroquine phosphate	$2.87 \cdot 10^{-2}$	4.0050
Tetracycline hydrochloride	$1.30 \cdot 10^{-10}$	0.0071

2.5. OPTIMIZATION PROCEDURE FOR FITTING CONCENTRATION-RESPONSE CURVES

There are four/five parameters that have to be calculated from toxicity data sets and then used to perform predictions. These are: r_{da}, and r_{ad} the exchange rates constants of uptake and depuration between the environment and the internal concentrations in 3T3, but they are both correlated; k_t, the killing rate constant for the mortality increase as a function of the chemical, the *NEC*, No-effect concentration for survival, which is the threshold concentration after which the toxic effects start, and, finally the decomposition (external to the cell)/metabolism(internal to the cell) rates, which were estimated as liquid and air half-lives times without metabolism. To obtain these parameters the integrated model, i.e. contaminant fate, cell population and toxicity effects, was run and the results compared with dose-response curves. Due to the absence of chemical concentration measurements during the experiments and to reduce the possibility of multiple minima, i.e. combination of parameters that would be able to simulate the same concentration-response curve (Zaldívar and Baraibar, 2011), the optimization was performed in two steps. In the first step disappearance rates from Table 3 and r_{da}, and r_{ad} from Table 5 and no-metabolism were used and only k_t, and *NEC* were optimized. Constrained optimization (only positive values) was carried out to minimize the error between modelled and fitted concentration-response curves using the Optimization Toolbox™ from MATLAB®. Afterwards all parameters were let to change and simulated annealing and genetic algorithms were used to explore the parameters' space followed by a constrained optimization when a plausible minimum was obtained.

3. RESULTS AND DISCUSSION

3.1. STAGE-BASED 3T3 CELL GROWTH MODEL

Since we are interested in coupling this model with a cell cycle model (e.g., Gérard and Goldbeter, 2009), the model was divided in four stages (phases) - G1, S, G2, M- corresponding to the cell cycle. Data in percentage on the duration in each stage for 3T3 was taken from Migita *et al*. (2010), d_{3T3} = [50.7, 19.2, 18.2, 11.9], whereas the total duration was taken as 19 h (Zaldívar *et al*., 2010). Mortalities were obtained from Kudryavtsev *et al*. (2004), z_i= [0.005, 0.005, 0.04, 0.04] (h^{-1}). *F* was considered as an optimization parameter.

Figure 6 shows the comparison between experimental growth data and model results (sum of all cells in the four stages). As can be observed 3T3 show an exponential growth during the duration of the experiment. These parameters were kept during the subsequent simulations.

Once we have a growth model of 3T3 cell lines and the model of the fate of the compound in the in vitro assay (Zaldívar et al., 2010), we can now try to simulate cell-based assays "*in silico*".

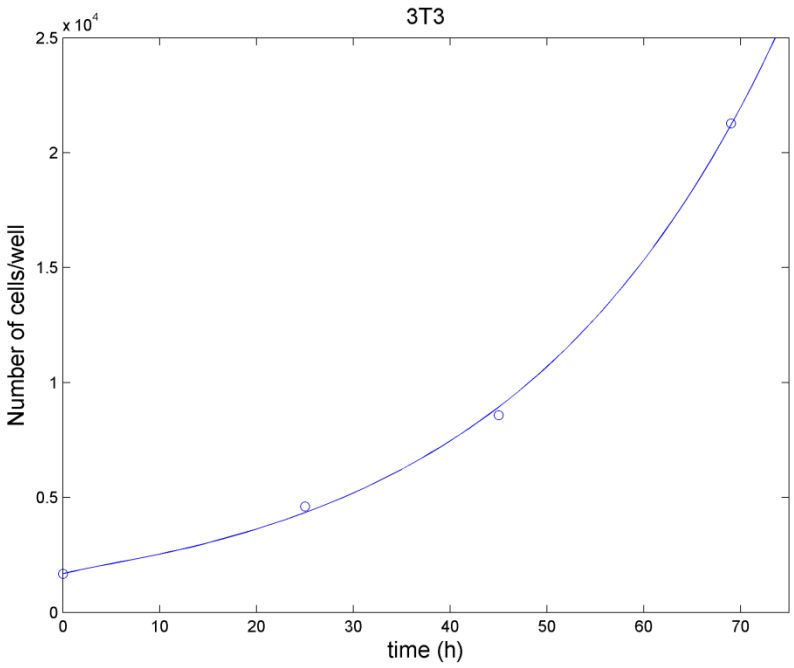

Figure 6. Simulated (continuous line) and experimental data on 3T3 cell population growth. Estimated 3T3 parameter: F=1.0261.

3.2. TOXICITY ASSAYS

3.2.1. Estimation of the killing rate and the no-effect concentration

Using the estimated values of r_{da} and the environmental degradation rates provided by EPI suite v4 (), we performed the fit of k_t and NEC. The optimization error was calculated as:

$$error = \sum_{i=1}^{n^o \exp} (Viability_{\exp.} - Viability_{sim.}) \qquad (36)$$

The obtained results are shown in Table 6, whereas in Figs. 7-26 the fitted concentration-response curves are shown, as well as the corresponding cell population dynamics and dissolved and internal concentrations. As it can be observed in Table 6, there are three compounds that have a high error after the optimization: Cycloheximide, Thioridazine hydrochloride and Colchicine, whereas for another two - Sodium lauryl sulfate and Amiodarone hydrochloride- the error is still high when compared with the rest of the compounds. For these five compounds we decided to perform an optimization including not only k_t and NEC, but also the rest of the model parameters estimated with empirical correlations or kept to zero due to the absence of data, i.e. decomposition reaction, uptake, depuration and metabolism rates. In any case looking at the concentration-response curves, it seems that in some cases there is a saturation of viability on the higher values of concentration. This effect may have a simpler explanation, i.e. solubility limit has been reached and therefore the nominal concentration in the system is, at these values, independent of the amount introduced in the system. However, solubility

data in pure water for Cycloheximide: 7.464 10^{-2} M (2 °C) and for Colchicine 1.088 10^{-1}M (25 °C) seem to contradict this explanation.

Table 6. Estimated k_t and *NEC* values and associated error for the selected chemicals.

Compound	k_t (s^{-1})	*NEC* (g gww^{-1})	*error*
Acetaminophen	2.20	$1.15 \cdot 10^{-3}$	190
Verapamil hydrochloride	18.55	$7.44 \cdot 10^{-3}$	0.3
Acetylsalicylic acid	$8.05 \cdot 10^{-2}$	$2.34 \cdot 10^{-2}$	91
Maprotiline	147.11	$1.44 \cdot 10^{-3}$	131
Cycloheximide	295.35	0	1218
Sodium lauryl sulfate	4.97	$8.24 \cdot 10^{-3}$	567
tert-Butyl hydroperoxide	38.55	$4.86 \cdot 10^{-3}$	139
Valproic acid	0.0567	$6.52 \cdot 10^{-2}$	34
Rifampin	1.16	$1.897 \cdot 10^{-2}$	62
Thioridazine hydrochloride	41.02	$0.905 \cdot 10^{-3}$	1210
Amiodarone hydrochloride	5.173	$2.943 \cdot 10^{-3}$	315
Caffeine	0.285	$6.944 \cdot 10^{-3}$	77
Carbamazepine	0.959	$9.696 \cdot 10^{-3}$	146
Colchicine	$1.505 \cdot 10^{3}$	$9.849 \cdot 10^{-7}$	1505
Acrylamide	1.89	$1.263 \cdot 10^{-3}$	106
Diphenhydramine	2.39	$4.258 \cdot 10^{-3}$	80
Pentachlorophenol	3.38	$1.893 \cdot 10^{-3}$	26
Disopyramide	1.77	$2.862 \cdot 10^{-3}$	93
Chloroquine diphosphate	24.66	$3.1967 \cdot 10^{-4}$	65
Tetracycline hydrochloride	471.94	$1.535 \cdot 10^{-6}$	134

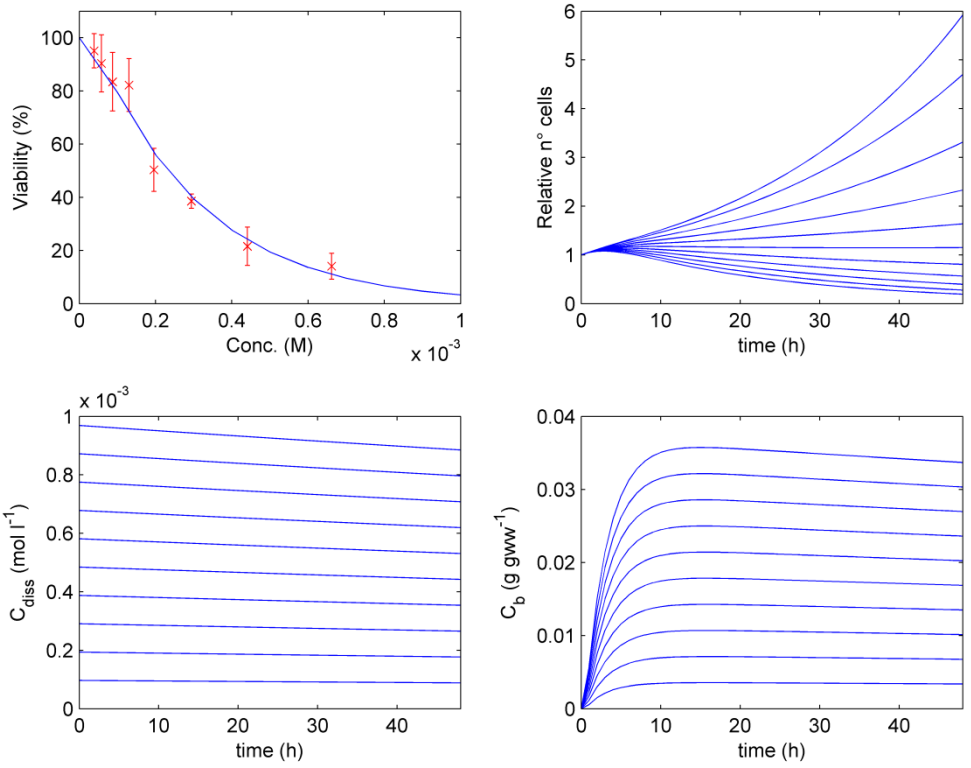

Figure 7. Acetaminophen. a/ Experimental and simulated concentration-response. For an increasing concentration between 0 and $1 \cdot 10^{-3}$ M ($0.1 \cdot 10^{-3}$ M steps): b/Relative number of living cells; c/ Dissolved concentration; d/ Internal concentration inside the cell.

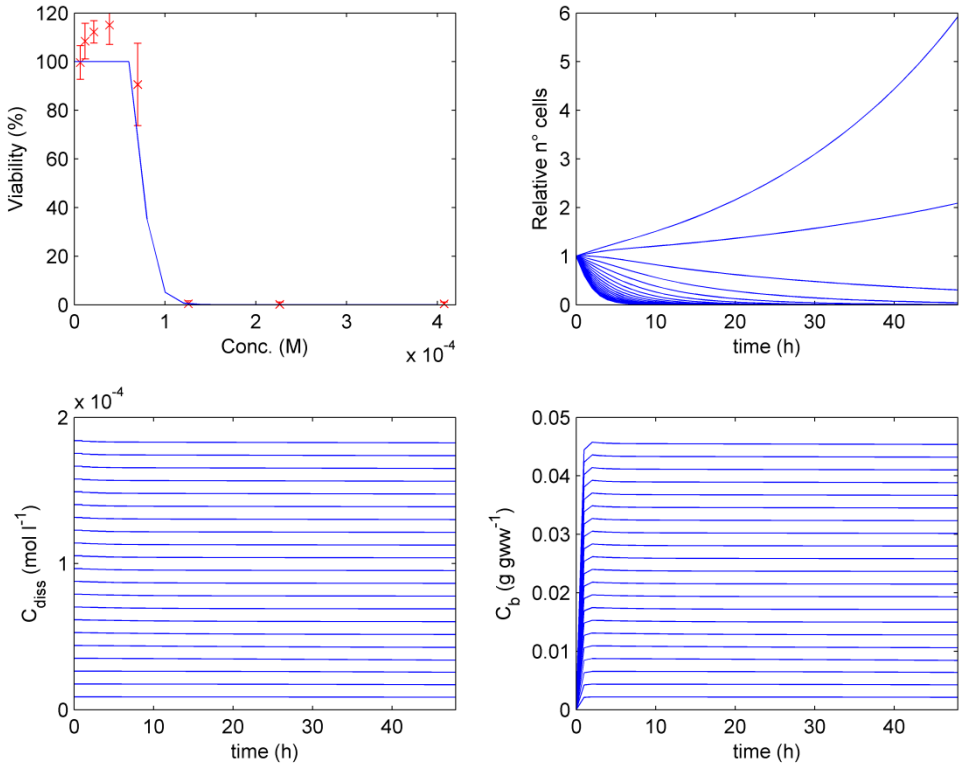

Figure 8. Verapamil hydrochloride. a/ Experimental and simulated concentration-response. For an increasing concentration between 0 and $4.2 \cdot 10^{-4}$ M ($0.2 \cdot 10^{-4}$ M steps): b/Relative number of living cells; c/ Dissolved concentration; d/ Internal concentration inside the cell.

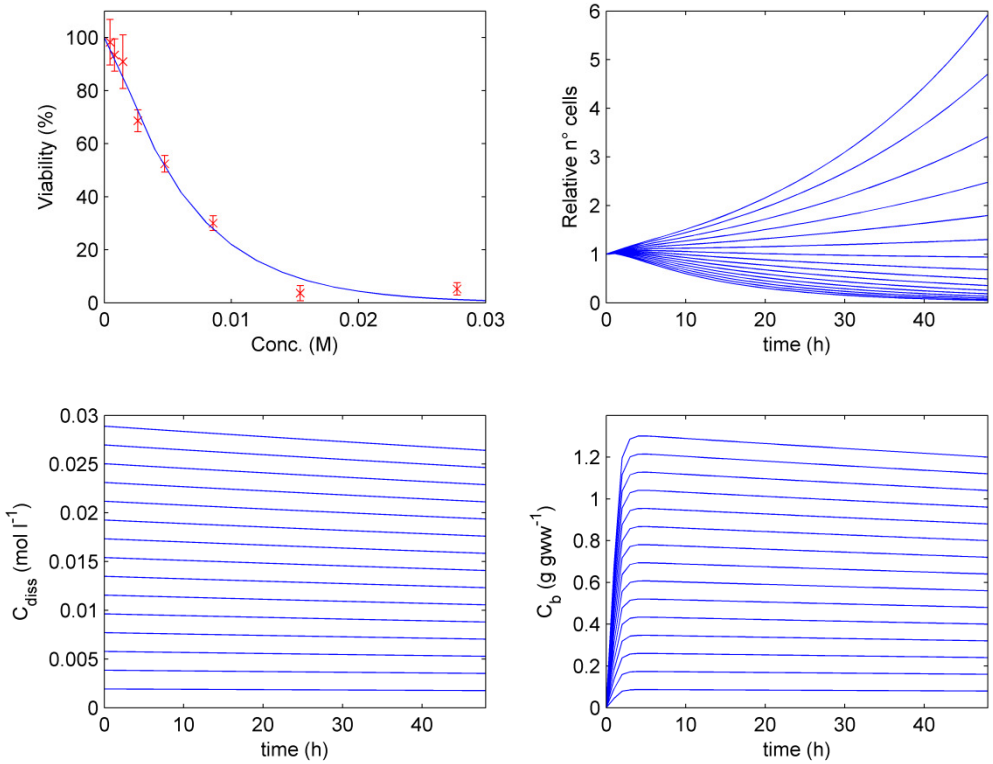

Figure 9. Acetylsalicylic acid. a/ Experimental and simulated concentration-response. For an increasing concentration between 0 and $3 \cdot 10^{-2}$ M ($0.2 \cdot 10^{-2}$ M steps): b/Relative number of living cells; c/ Dissolved concentration; d/ Internal concentration inside the cell.

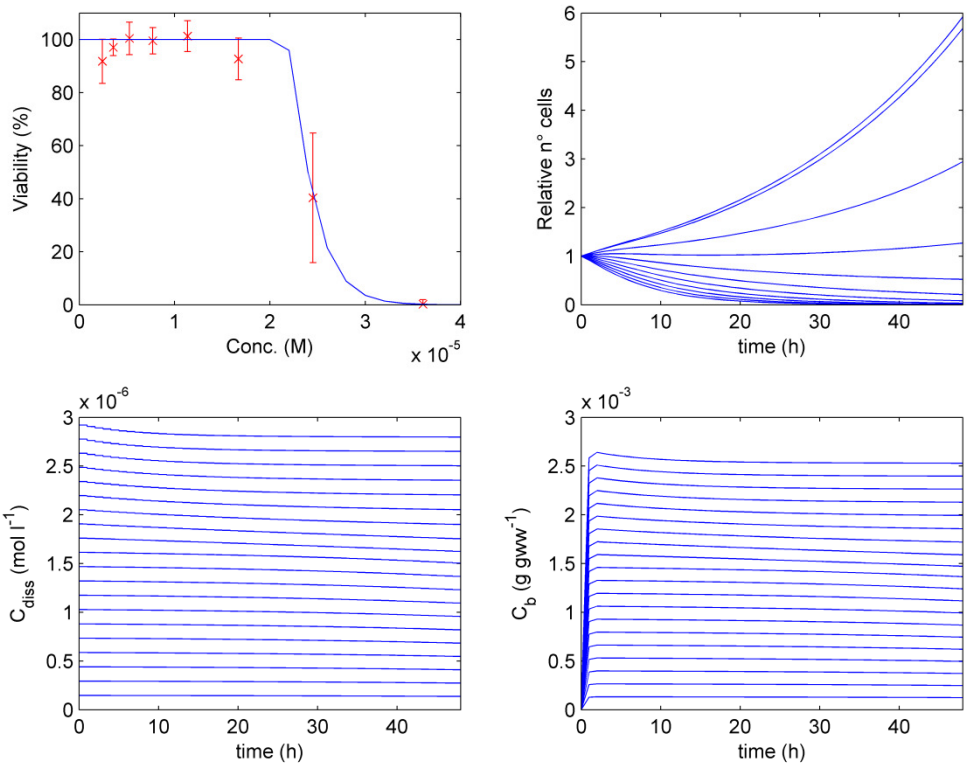

Figure 10. Maprotiline. a/ Experimental and simulated concentration-response. For an increasing concentration between 0 and $5 \cdot 10^{-3}$ M (0.2 M steps): b/Relative number of living cells; c/ Dissolved concentration; d/ Internal concentration inside the cell.

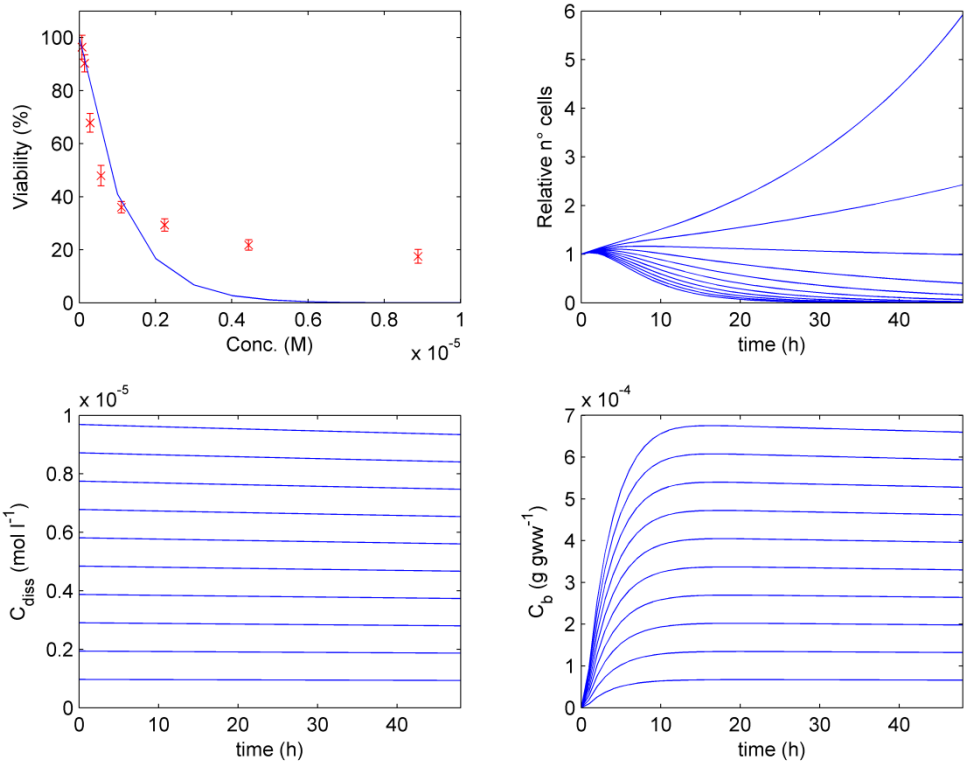

Figure 11. Cycloheximide. a/ Experimental and simulated concentration-response. For an increasing concentration between 0 and $5 \cdot 10^{-3}$ M (0.2 M steps): b/Relative number of living cells; c/ Dissolved concentration; d/ Internal concentration inside the cell.

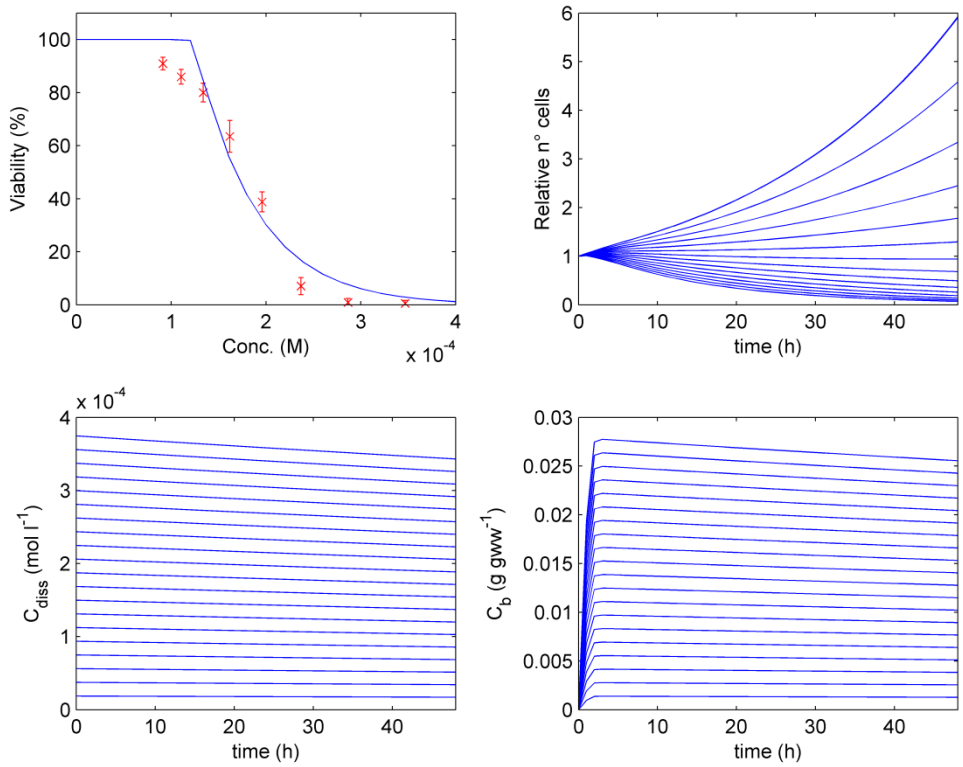

Figure 12. Sodium lauryl sulfate. a/ Experimental and simulated concentration-response. For an increasing concentration between 0 and $5 \cdot 10^{-3}$ M (0.2 M steps): b/Relative number of living cells; c/ Dissolved concentration; d/ Internal concentration inside the cell.

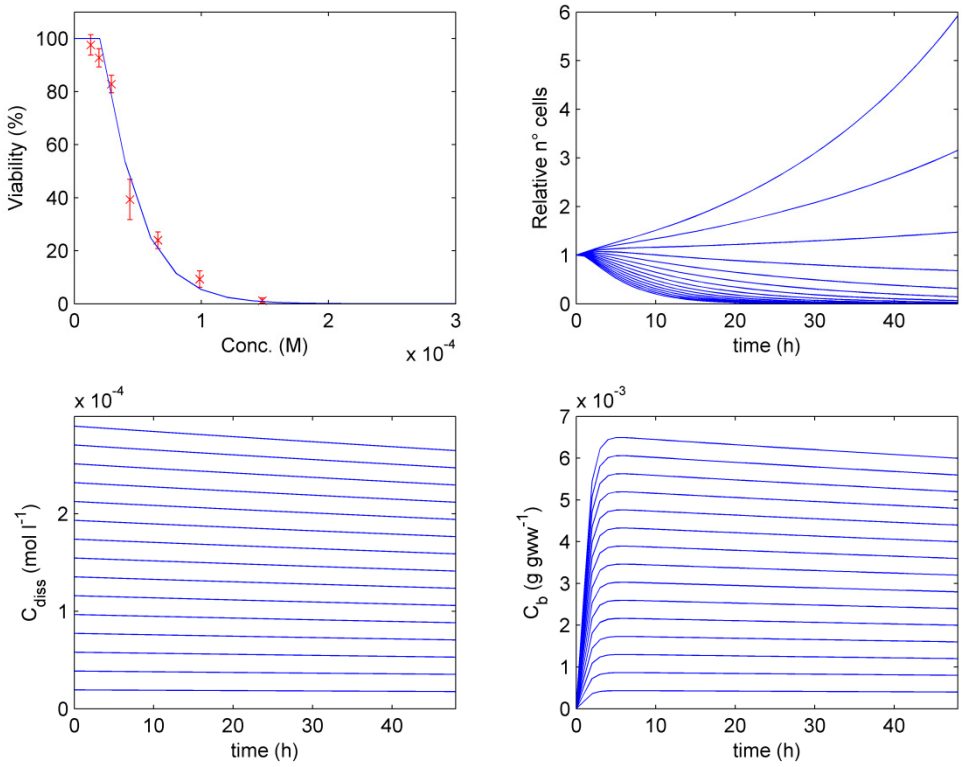

Figure 13. tert-Butyl hydroperoxide. a/ Experimental and simulated concentration-response. For an increasing concentration between 0 and $3 \cdot 10^{-4}$ M ($0.2 \cdot 10^{-4}$ M steps): b/Relative number of living cells; c/ Dissolved concentration; d/ Internal concentration inside the cell.

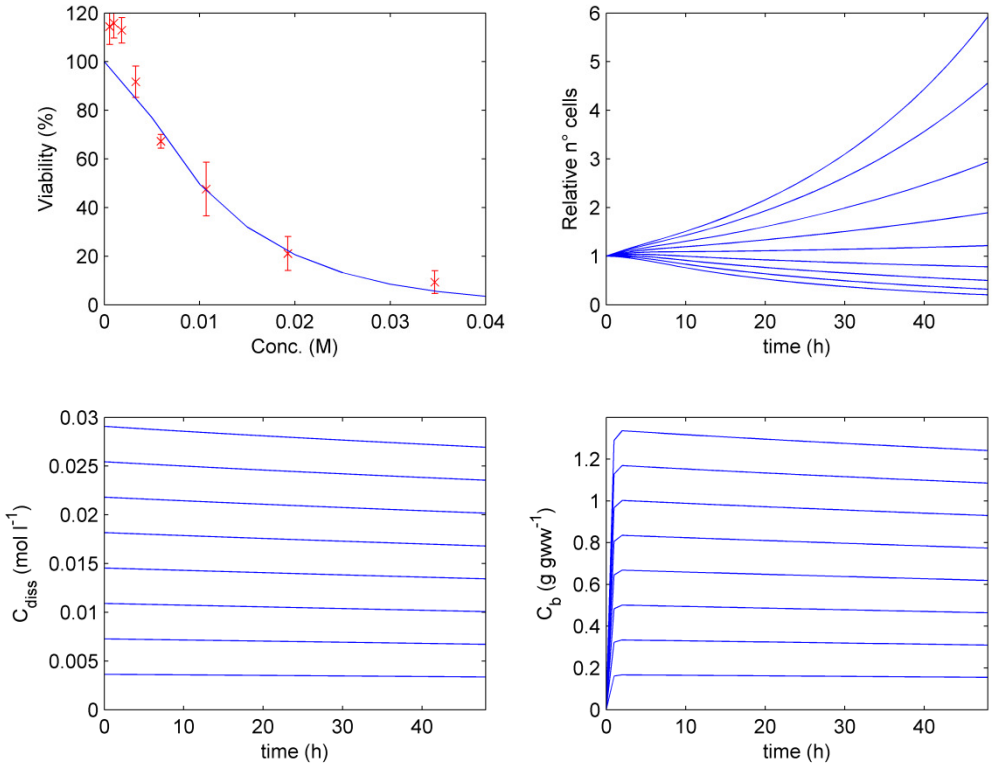

Figure 14. Valproic acid. a/ Experimental and simulated concentration-response. For an increasing concentration between 0 and $4 \cdot 10^{-2}$ M ($0.5 \cdot 10^{-2}$ M steps): b/Relative number of living cells; c/ Dissolved concentration; d/ Internal concentration inside the cell.

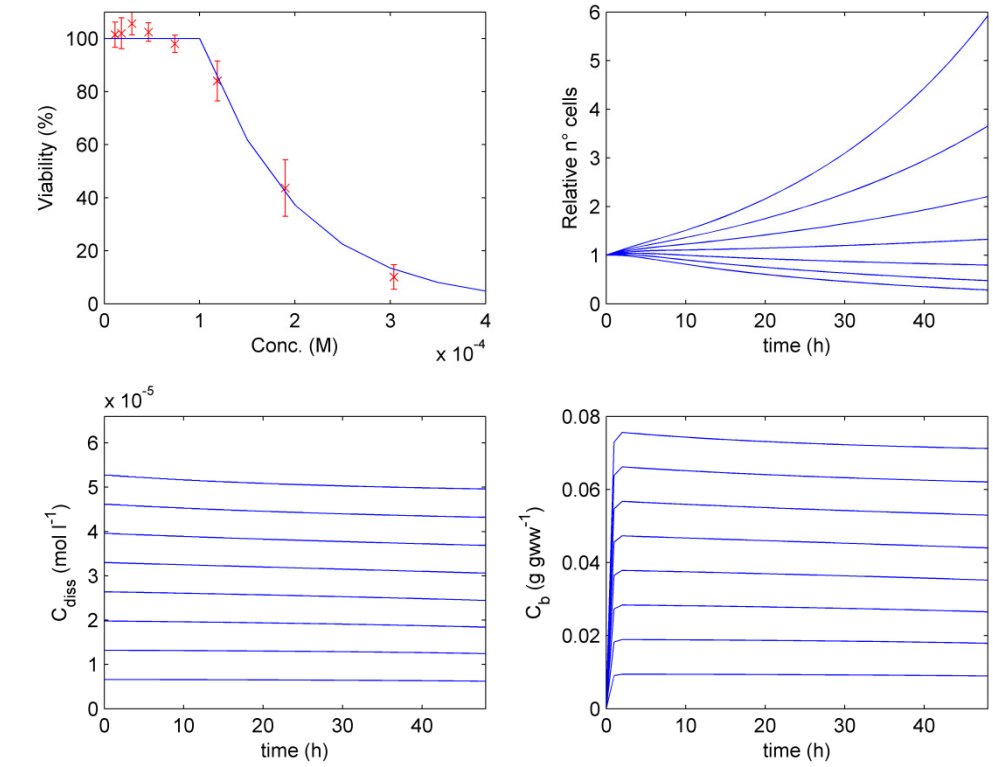

Figure 15. Rifampin. a/ Experimental and simulated concentration-response. For an increasing concentration between 0 and $4 \cdot 10^{-4}$ M ($0.5 \cdot 10^{-4}$ M steps): b/Relative number of living cells; c/ Dissolved concentration; d/ Internal concentration inside the cell.

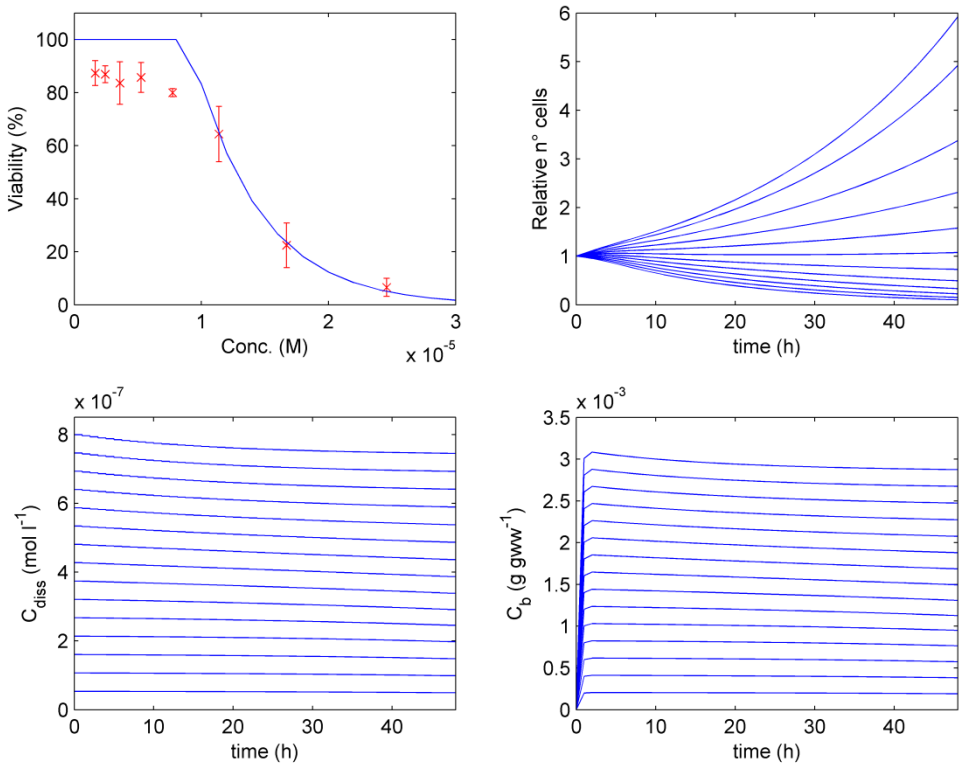

Figure 16. Thioridazine hydrochloride. a/ Experimental and simulated concentration-response. For an increasing concentration between 0 and $3 \cdot 10^{-5}$ M ($0.2 \cdot 10^{-5}$ M steps): b/Relative number of living cells; c/ Dissolved concentration; d/ Internal concentration inside the cell.

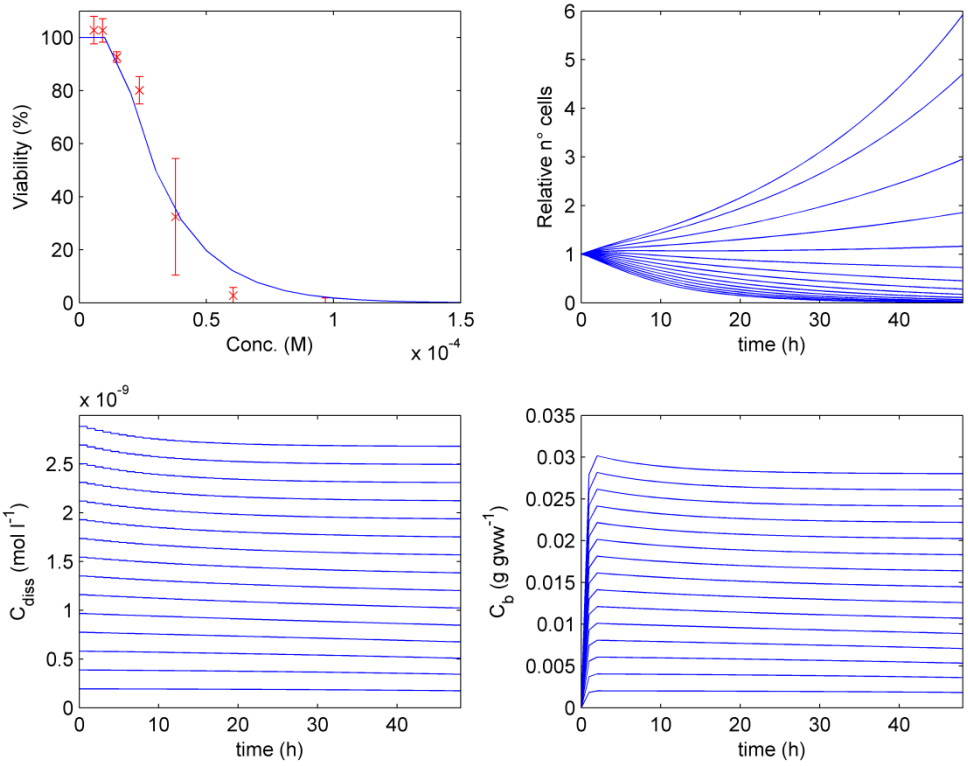

Figure 17. Amiodarone hydrochloride. a/ Experimental and simulated concentration-response. For an increasing concentration between 0 and $1.5 \cdot 10^{-4}$ M ($0.1 \cdot 10^{-4}$ M steps): b/Relative number of living cells; c/ Dissolved concentration; d/ Internal concentration inside the cell.

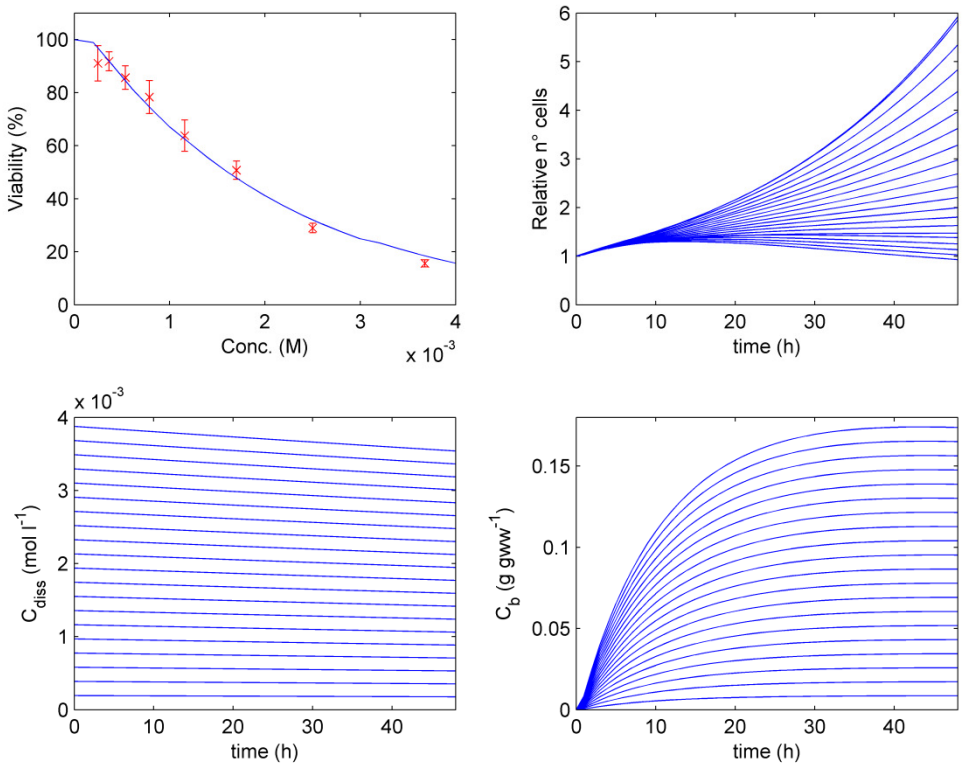

Figure 18. Caffeine. a/ Experimental and simulated concentration-response. For an increasing concentration between 0 and $4 \cdot 10^{-3}$ M ($0.2 \cdot 10^{-3}$ M steps): b/Relative number of living cells; c/ Dissolved concentration; d/ Internal concentration inside the cell.

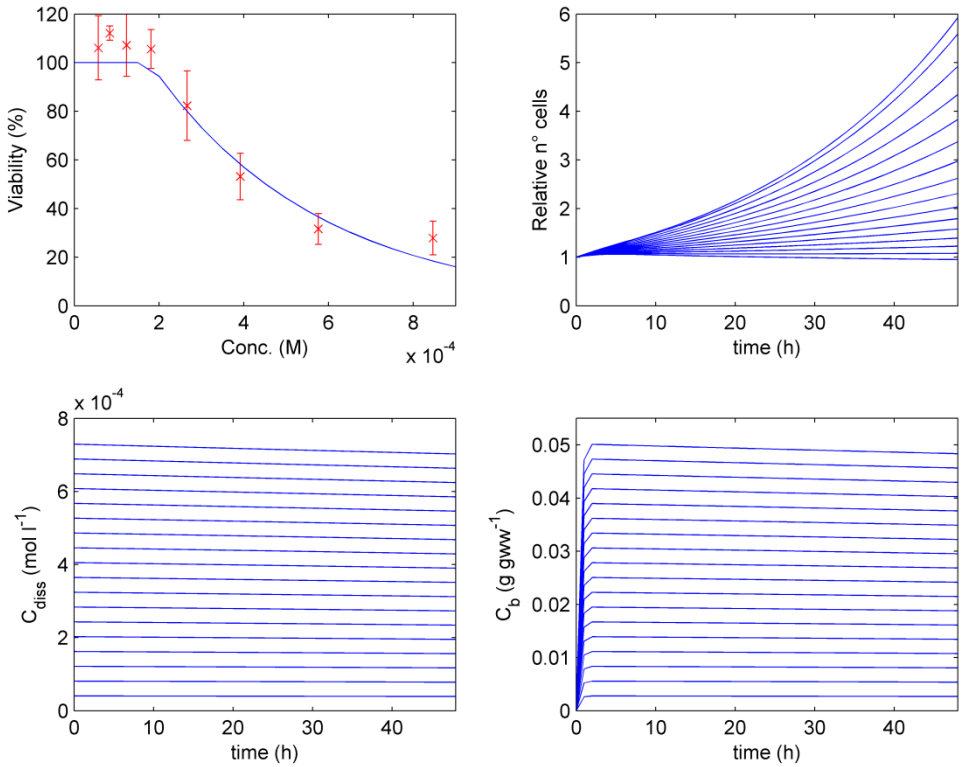

Figure 19. Carbamazepine. a/ Experimental and simulated concentration-response. For an increasing concentration between 0 and $9 \cdot 10^{-4}$ M ($0.5 \cdot 10^{-4}$ M steps): b/Relative number of living cells; c/ Dissolved concentration; d/ Internal concentration inside the cell.

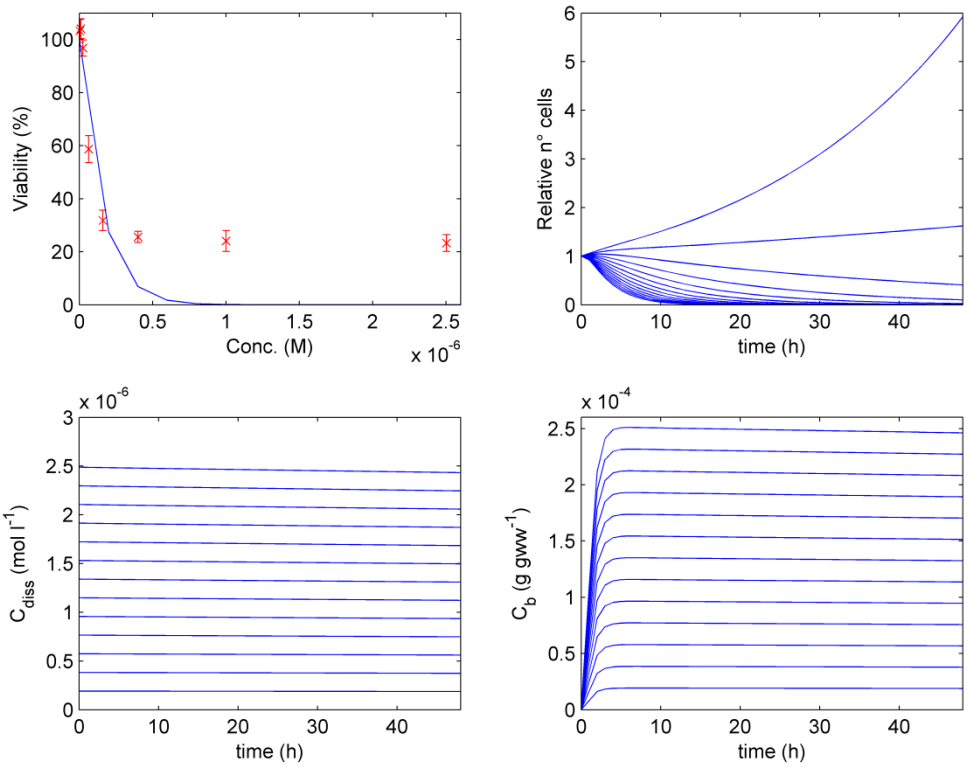

Figure 20. Colchicine. a/ Experimental and simulated concentration-response. For an increasing concentration between 0 and $2.6 \cdot 10^{-6}$ M ($0.2 \cdot 10^{-6}$ M steps): b/Relative number of living cells; c/ Dissolved concentration; d/ Internal concentration inside the cell.

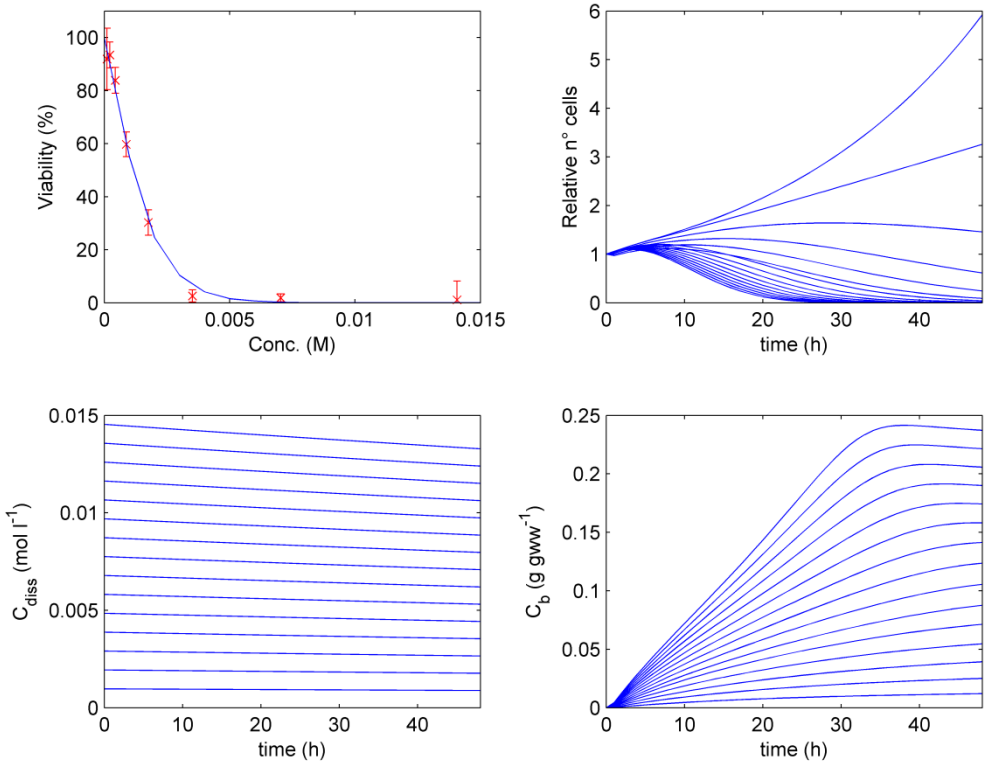

Figure 21. Acrylamide. a/ Experimental and simulated concentration-response. For an increasing concentration between 0 and $15 \cdot 10^{-3}$ M ($1 \cdot 10^{-3}$ M steps): b/Relative number of living cells; c/ Dissolved concentration; d/ Internal concentration inside the cell.

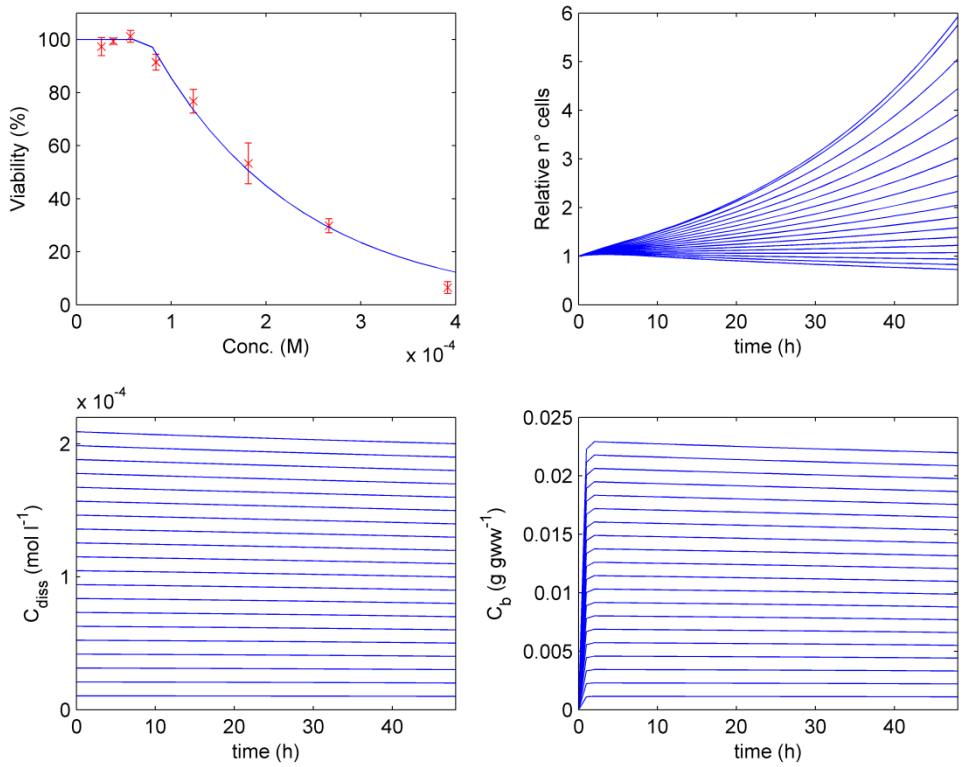

Figure 22. Diphenhydramine. a/ Experimental and simulated concentration-response. For an increasing concentration between 0 and $4 \cdot 10^{-3}$ M ($0.2 \cdot 10^{-3}$ M steps): b/Relative number of living cells; c/ Dissolved concentration; d/ Internal concentration inside the cell.

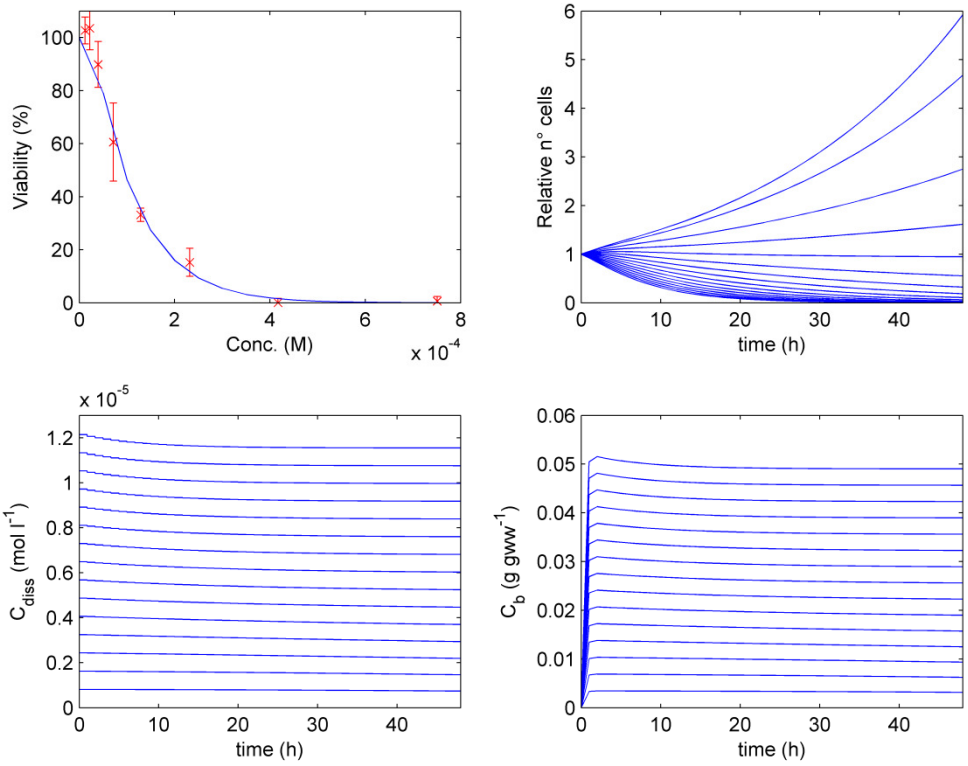

Figure 23. Pentachlorophenol. a/ Experimental and simulated concentration-response. For an increasing concentration between 0 and $7.5 \cdot 10^{-4}$ M ($0.5 \cdot 10^{-4}$ M steps): b/Relative number of living cells; c/ Dissolved concentration; d/ Internal concentration inside the cell.

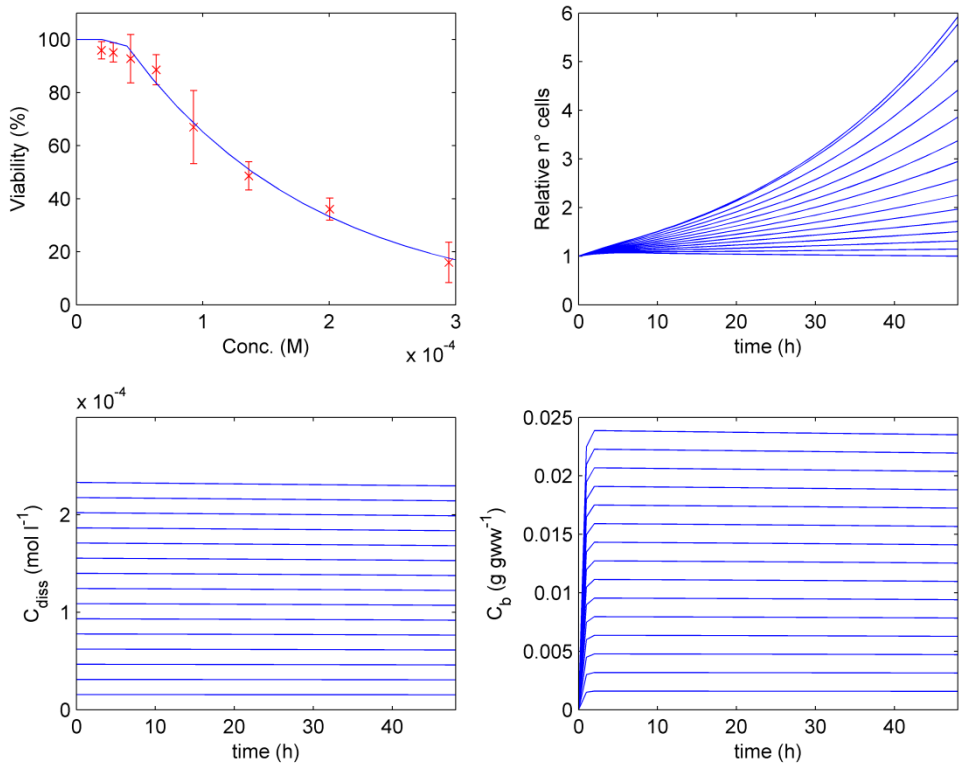

Figure 24. Disopyramide. a/ Experimental and simulated concentration-response. For an increasing concentration between 0 and $3 \cdot 10^{-4}$ M ($0.2 \cdot 10^{-4}$ M steps): b/Relative number of living cells; c/ Dissolved concentration; d/ Internal concentration inside the cell.

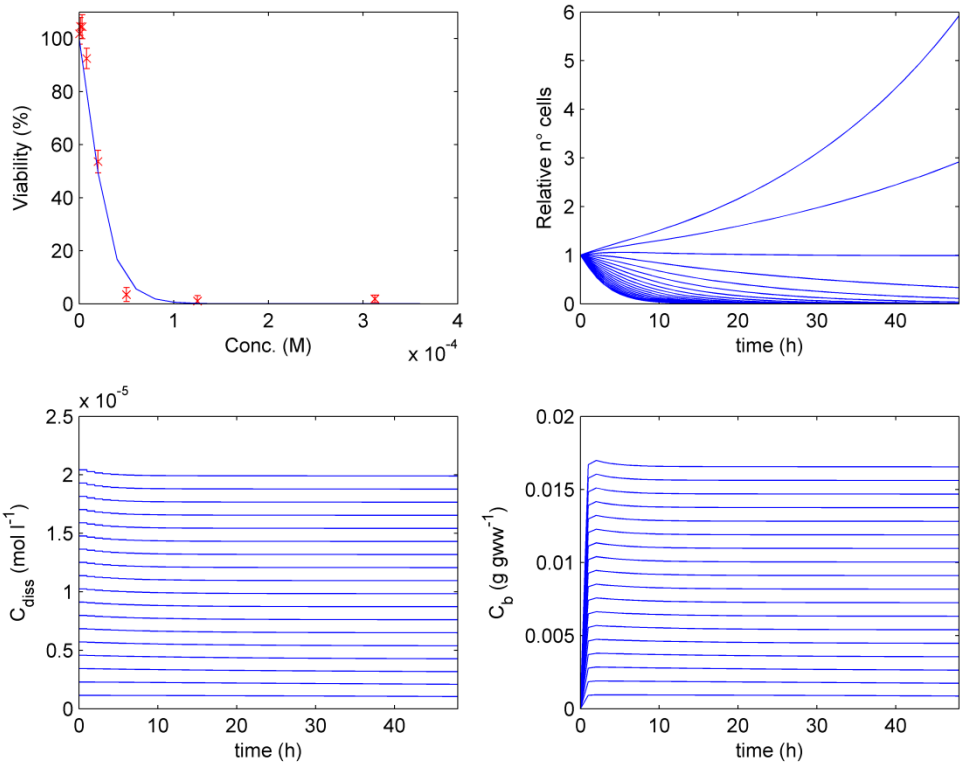

Figure 25. Chloroquine diphosphate. a/ Experimental and simulated concentration-response. For an increasing concentration between 0 and $3.6 \cdot 10^{-4}$ M ($0.2 \cdot 10^{-4}$ M steps): b/Relative number of living cells; c/ Dissolved concentration; d/ Internal concentration inside the cell.

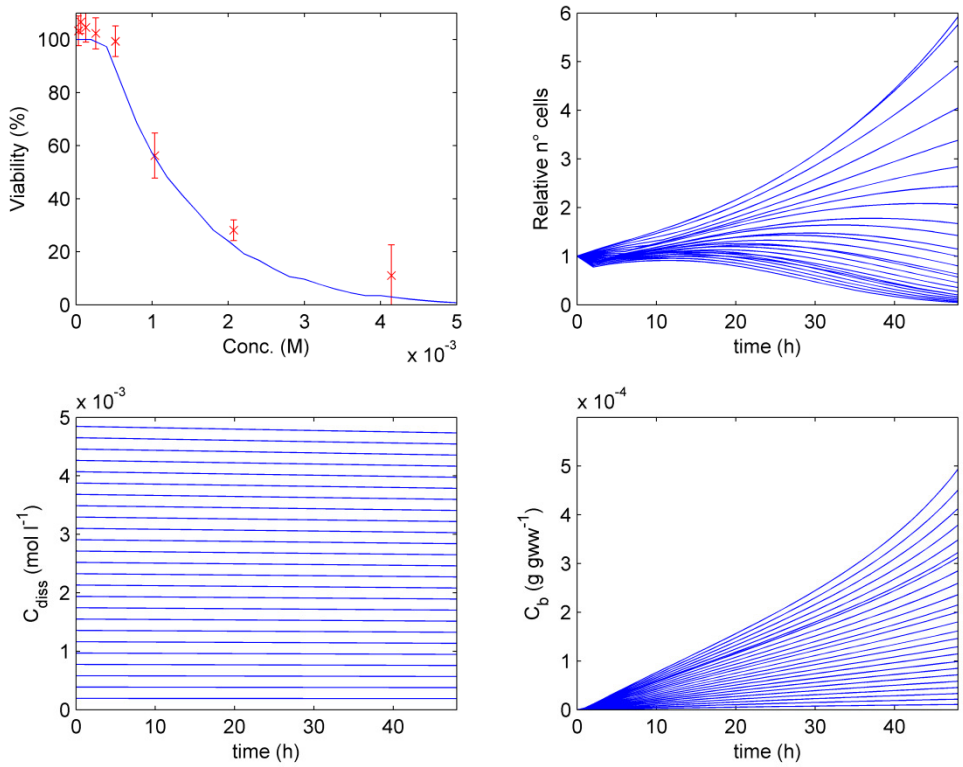

Figure 26. Tetracycline hydrochloride. a/ Experimental and simulated concentration-response curve. For an increasing concentration between 0 and $5 \cdot 10^{-3}$ M ($0.2 \cdot 10^{-3}$ M steps): b/Relative number of living cells; c/ Dissolved concentration; d/ Internal concentration inside the cell.

Due to the different physico-chemical properties of the twenty studied compounds, the dynamics of dissolved and internal concentrations changes appreciably from experiment to experiment. Concerning dissolved concentrations, it is possible to observe the differences in scale between the nominal concentration in the concentration-response curves and the dissolved concentrations time series. For hydrophilic compounds there is practically no difference, e.g., Caffeine in Fig. 18; whereas for hydrophobic compounds the differences increase reaching up to several orders of magnitude, see for example Fig. 17 for Amiodarone. In addition, it is also possible to observe for several compounds the role of decomposition reactions in the decrease of concentration over time. However, all these values should be checked with experimental data to confirm the right amount of these reactions since the medium is not comparable with environmental half lives we have used to implement the model. Concerning internal concentrations, hydrophobic compounds tend to reach saturation quite rapidly, whereas for hydrophilic compounds the time need is longer, being Tetracycline the extreme case where after 48 hours internal concentrations have not reach the saturation concentration yet. For two cases: Valproic and Acetylsalicylic acid, internal concentrations reach too high values to assume that no saturation occurs, therefore, at these values probably all correlations are not valid anymore.

Table 7 summarizes the main results obtained using a nominal concentration corresponding to the IC_{50} value concerning dissolved and internal concentrations and their respective areas under the curve (AUC).

Table 7. Calculated average values of C_{diss}, C_b and the respective areas under the curve (AUC) for the selected chemicals at their IC_{50} nominal concentrations.

Compound	C_{diss} (mol l^{-1})	C_b (g gww^{-1})	AUC_{diss} (mol h l^{-1})	AUC_b(g h gww^{-1})
Acetaminophen	$2.03 \cdot 10^{-4}$	$7.1 \cdot 10^{-3}$	$9.7 \cdot 10^{-3}$	0.384
Verapamil hydrochloride	$3.41 \cdot 10^{-5}$	$8.3 \cdot 10^{-3}$	$1.6 \cdot 10^{-3}$	0.407
Acetylsalicylic acid	$4.3 \cdot 10^{-3}$	$1.9 \cdot 10^{-1}$	$2.1 \cdot 10^{-1}$	9.245
Maprotiline	$1.65 \cdot 10^{-6}$	$1.5 \cdot 10^{-3}$	$7.93 \cdot 10^{-5}$	0.072
Cycloheximide	$5.75 \cdot 10^{-7}$	$3.71 \cdot 10^{-5}$	$2.76 \cdot 10^{-5}$	0.002
Sodium lauryl sulfate	$1.55 \cdot 10^{-4}$	$1.12 \cdot 10^{-2}$	$7.4 \cdot 10^{-3}$	0.550
tert-Butyl hydroperoxide	$3.88 \cdot 10^{-5}$	$8.46 \cdot 10^{-4}$	$1.9 \cdot 10^{-3}$	0.041
Valproic acid	$6.6 \cdot 10^{-3}$	$2.99 \cdot 10^{-1}$	$3.18 \cdot 10^{-1}$	14.656
Rifampin	$2.27 \cdot 10^{-5}$	$3.2 \cdot 10^{-2}$	$1.1 \cdot 10^{-3}$	1.567
Thioridazine hydrochloride	$2.76 \cdot 10^{-7}$	$1.0 \cdot 10^{-3}$	$1.32 \cdot 10^{-5}$	0.051
Amiodarone hydrochloride	$5.84 \cdot 10^{-10}$	$6.0 \cdot 10^{-3}$	$2.80 \cdot 10^{-8}$	0.293
Caffeine	$1.5 \cdot 10^{-3}$	$5.69 \cdot 10^{-2}$	$7.38 \cdot 10^{-2}$	2.778
Carbamazepine	$3.23 \cdot 10^{-4}$	$2.17 \cdot 10^{-2}$	$1.55 \cdot 10^{-2}$	1.066
Colchicine	$8.66 \cdot 10^{-8}$	$8.44 \cdot 10^{-6}$	$4.16 \cdot 10^{-6}$	$4.13 \cdot 10^{-4}$
Acrylamide	$1.0 \cdot 10^{-3}$	$8.6 \cdot 10^{-3}$	$4.94 \cdot 10^{-2}$	0.419
Diphenhydramine	$9.37 \cdot 10^{-5}$	$1.01 \cdot 10^{-2}$	$4.5 \cdot 10^{-3}$	0.494
Pentachlorophenol	$1.45 \cdot 10^{-6}$	$6.0 \cdot 10^{-3}$	$6.95 \cdot 10^{-5}$	0.296
Disopyramide	$1.07 \cdot 10^{-4}$	$1.07 \cdot 10^{-2}$	$5.2 \cdot 10^{-3}$	0.527
Chloroquine diphosphate	$1.14 \cdot 10^{-6}$	$9.33 \cdot 10^{-4}$	$5.49 \cdot 10^{-5}$	0.046
Tetracycline hydrochloride	$1.1 \cdot 10^{-3}$	$3.53 \cdot 10^{-5}$	$5.43 \cdot 10^{-2}$	0.002

3.2.2. Global estimation of model's parameters

To improve the parameter's optimization for the compounds with the highest error, see Table 6, we decided, in addition to k_t and NEC for which correlations or no value has been provided, to free the rest of parameters. These are: r_{da} and r_{ad}, k_{deg} and k_{met}. The results obtained are summarized in Table 8. As one would expect, as the number of parameters increases, the optimization errors tend to decrease. However, multiple minima where found which implies that the concentration-response curves alone are not enough to elucidate which is the best set of parameters that will fit the data, and concentration measurements become critical to validate the model. Therefore, even though we are able to fit the experimental data, the system is not completely observable with only the available experimental data and we cannot be certain that the simulated values of dissolved and internal concentrations are correct.

Table 8. Estimated r_{da}, k_{deg}, k_{met}, k_t and NEC values and associated error for the selected chemicals.

Compound	r_{da}(l cm^{-2} s^{-1})	k_{deg} (s^{-1})	k_{met} (s^{-1})	k_t (s^{-1})	NEC (g gww^{-1})	error
Cycloheximide	$0.686 \cdot 10^{-3}$	$2.34 \cdot 10^{-2}$	0	$1.46 \cdot 10^{3}$	0	531
Sodium lauryl sulfate	$2.93 \cdot 10^{-5}$	$7.25 \cdot 10^{-6}$	$2.18 \cdot 10^{-5}$	13.52	$6.76 \cdot 10^{-3}$	205
Thioridazine hydrochloride	$3.704 \cdot 10^{-3}$	$2.33 \cdot 10^{-3}$	$1.68 \cdot 10^{-6}$	175.87	$1.41 \cdot 10^{-4}$	775
Amiodarone hydrochloride	0.252	$1.68 \cdot 10^{-6}$	$4.04 \cdot 10^{-4}$	32.11	$6.64 \cdot 10^{-4}$	71
Colchicine	$5.552 \cdot 10^{-5}$	1.035	0	$2.49 \cdot 10^{7}$	0	974

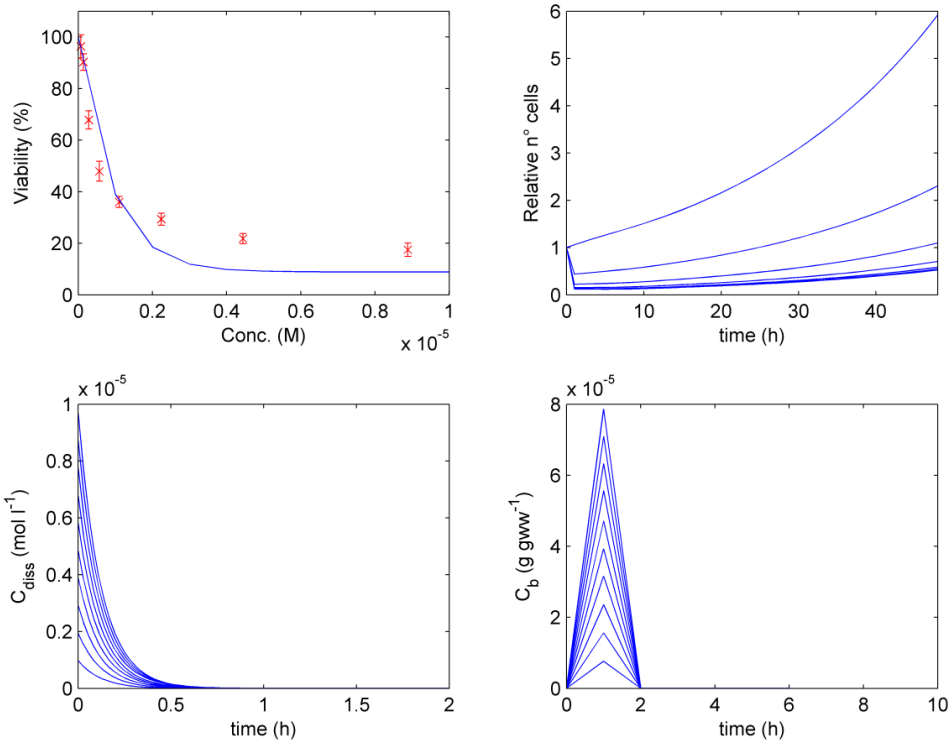

Figure 27. Cycloheximide. a/ Experimental and simulated concentration-response curve. For an increasing concentration between 0 and $5 \cdot 10^{-3}$ M ($0.2 \cdot 10^{-3}$ M steps): b/Relative number of living cells; c/ Dissolved concentration; d/ Internal concentration inside the cell (with the obtained parameters, the compound disappears rapidly from the well).

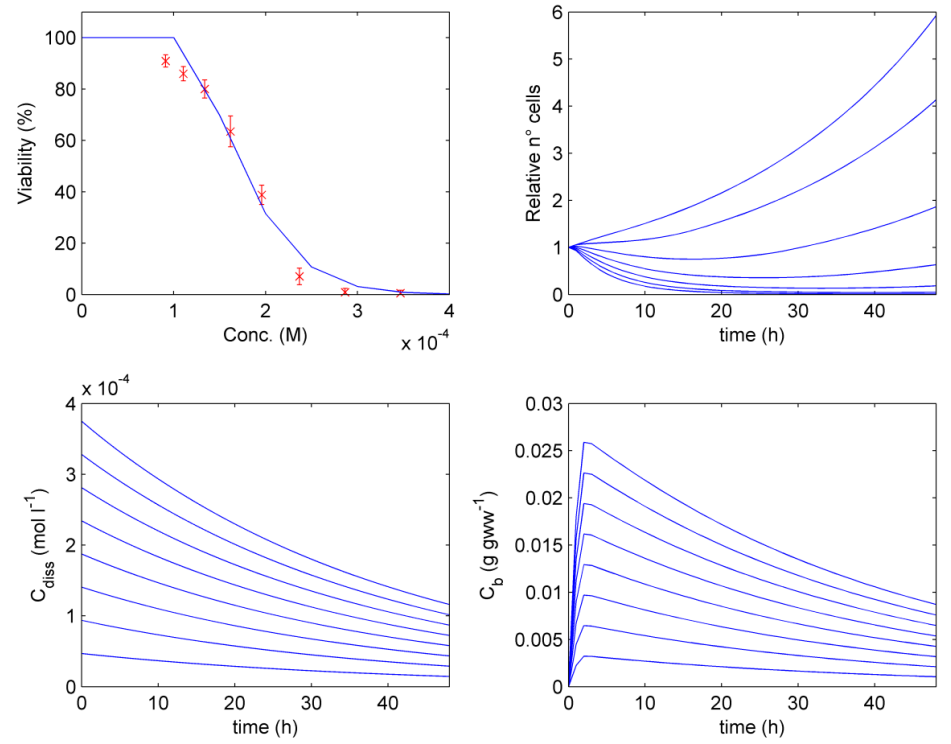

Figure 28. Sodium lauryl sulfate. a/ Experimental and simulated concentration-response curve. For an increasing concentration between 0 and $4 \cdot 10^{-4}$ M ($0.5 \cdot 10^{-4}$ M steps): b/Relative number of living cells; c/ Dissolved concentration; d/ Internal concentration inside the cell.

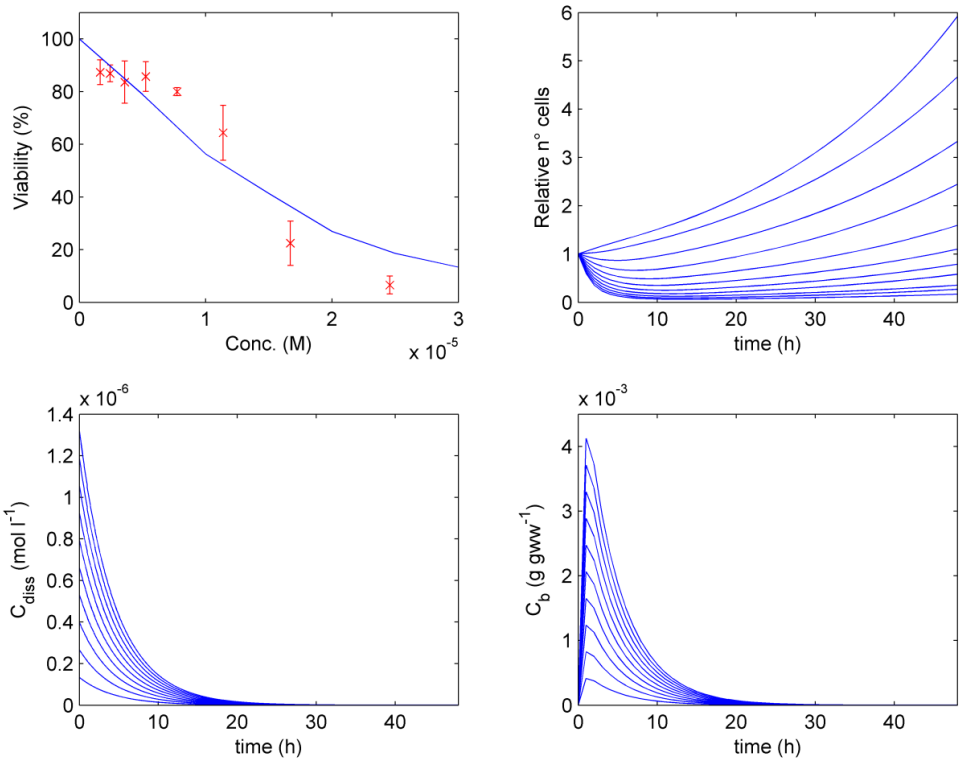

Figure 29. Thioridazine hydrochloride. a/ Experimental and simulated concentration-response curve. For an increasing concentration between 0 and $3 \cdot 10^{-5}$ M ($0.5 \cdot 10^{-5}$ M steps): b/Relative number of living cells; c/ Dissolved concentration; d/ Internal concentration inside the cell.

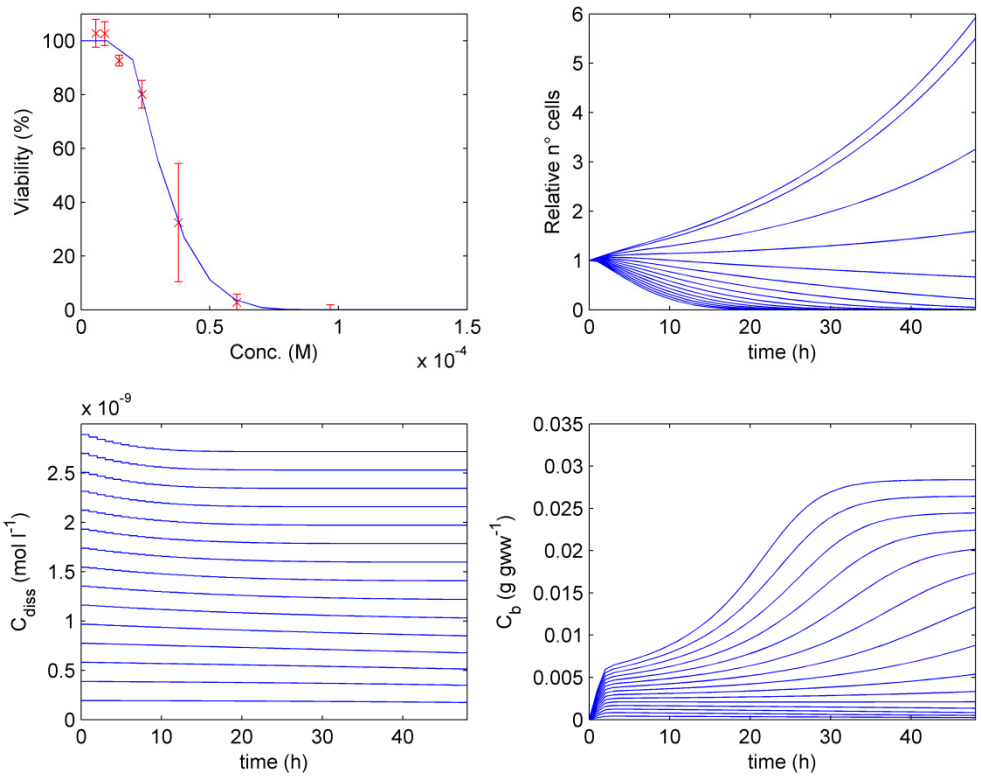

Figure 30. Amiodarone hydrochloride. a/ Experimental and simulated concentration-response curve. For an increasing concentration between 0 and $1.5 \cdot 10^{-4}$ M ($0.1 \cdot 10^{-4}$ M steps): b/Relative number of living cells; c/ Dissolved concentration; d/ Internal concentration inside the cell.

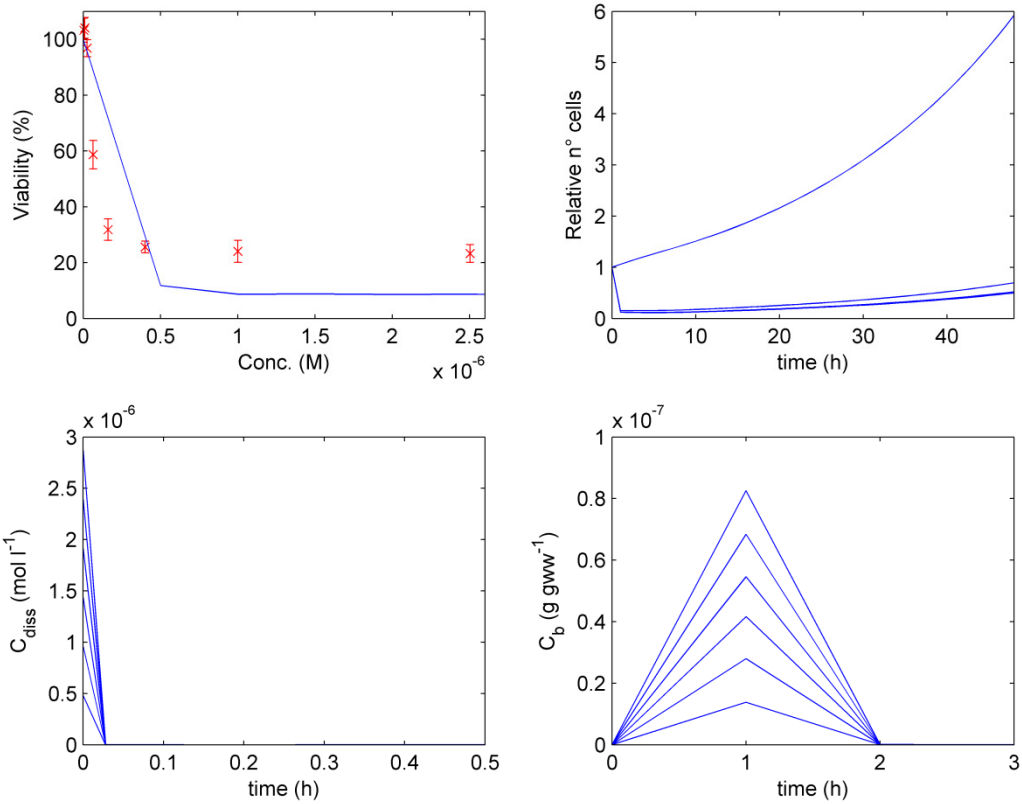

Figure 31. Colchicine. a/ Experimental and simulated concentration-response curve. For an increasing concentration between 0 and $3.0 \cdot 10^{-6}$ M ($0.5 \cdot 10^{-6}$ M steps): b/Relative number of living cells; c/ Dissolved concentration; d/ Internal concentration inside the cell.

The results after the optimization of all these parameters point out to the fact that only viability data at 48 h is not enough to properly validate the model and to have a precise idea of free and internal concentrations. It is necessary to anchor chemical concentrations with experimental data to be able to obtain reliable model's parameters. Specifically, for cycloheximide and colchicine, better fits are obtained assuming fast degradation since the viability seems to reach a constant value at higher concentrations.

3.2.3. Simulation of the cell population experiments

Even though we tried to keep similar conditions to the 3T3 experiments carried out in the HTS laboratory, the field imaging microscopy experiment did not show the same growth rates as the initial growth experiment, see Fig. 6. For this reason, we decided to change only the *F* value to approximate the growth values in the control experiment, but kept the same parameters of the toxicity model. Figure 32 shows the experimental versus simulated results. As it can be observed the model tends to predict a higher mortality and therefore a fast decrease in cell population. However the results are satisfactory in view of the viability variability between duplicates observed during the experiments, see Figs. 3-4.

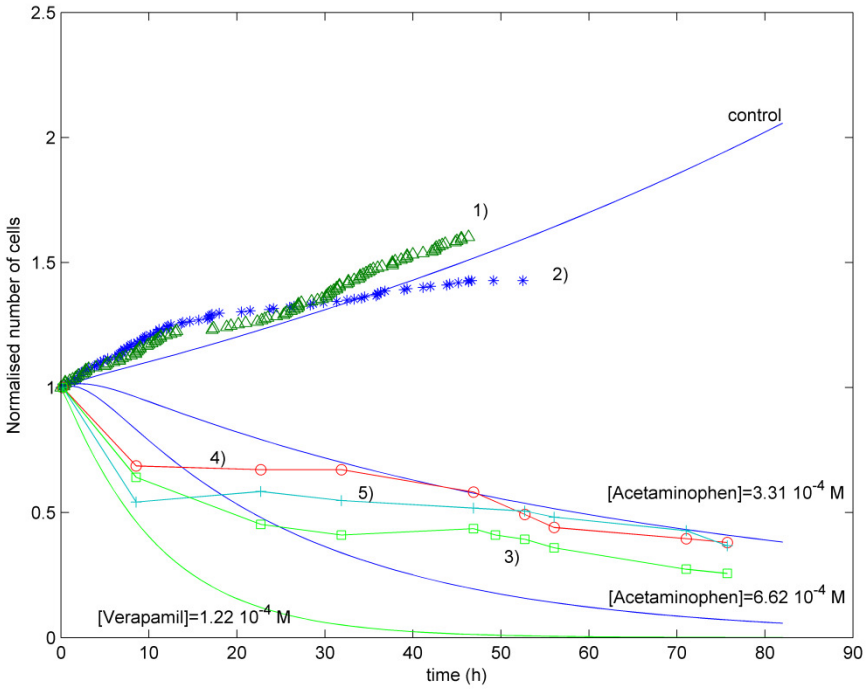

Figure 32. Experimental versus simulated cell population dynamics. Only the fecundity parameter *F* was modified (*F*=0.65) to adjust the growth in the two control experiments: 1) and 2). 3) Addition of Verapamil $1.22 \cdot 10^{-4}$M; 4) addition of Acetaminophen $3.31 \cdot 10^{-4}$M and 5) addition of Acetaminophen $6.62 \cdot 10^{-4}$M.

3.3. *IN VITRO – IN VIVO* EXTRAPOLATION

On of the objectives for the development of a cell-based assay model was to develop a system able to calculate the concentrations that the cell experience, i.e., the free/unbound concentration, and also to estimate the internal concentrations inside the cell. In this sense it is possible to express the obtained IC_{50} as IC_{50}^{free} and the internal concentrations at IC_{50} as IC_{50}^{int}, and check if these values are better predictive tools for the in vivo LD_{50}. In any case, in the future we plan to correlate these values with the corresponding values provided by a PBTK (Physiologically based toxicokinetic) model, correcting, or providing free and internal concentrations *in vivo*. This would allow comparing the "same" values. In this work, we are only able to provide a correction for the x-axis in the plot IC_{50}-LD_{50}.

As it is already well-know, the comparison between IC_{50} and LD_{50} (see Fig. 33) provides a low correlation value, r^2=0.505, for the twenty analysed compounds. The results obtained using the values of dissolved, internal and their respective areas under the curve (AUC) in Table 7 have been compared with the LD_{50} values (see Fig. 34); however, the r^2 correlation values obtained does not improve the value obtained by the direct comparison between IC_{50} and LD_{50}, i.e., 0.19 for C_{diss}, 0.25 for C_b, 0.19 for AUC_{diss}, 0.25 for AUC_b. There are two plausible explanations for these results, the first is that the concentrations predicted by the model are not correct -see the results and discussion in Section 3.2.-,

the second is that the conversion *in vivo* is still missing and therefore we should correct also the y-axis in the plots.

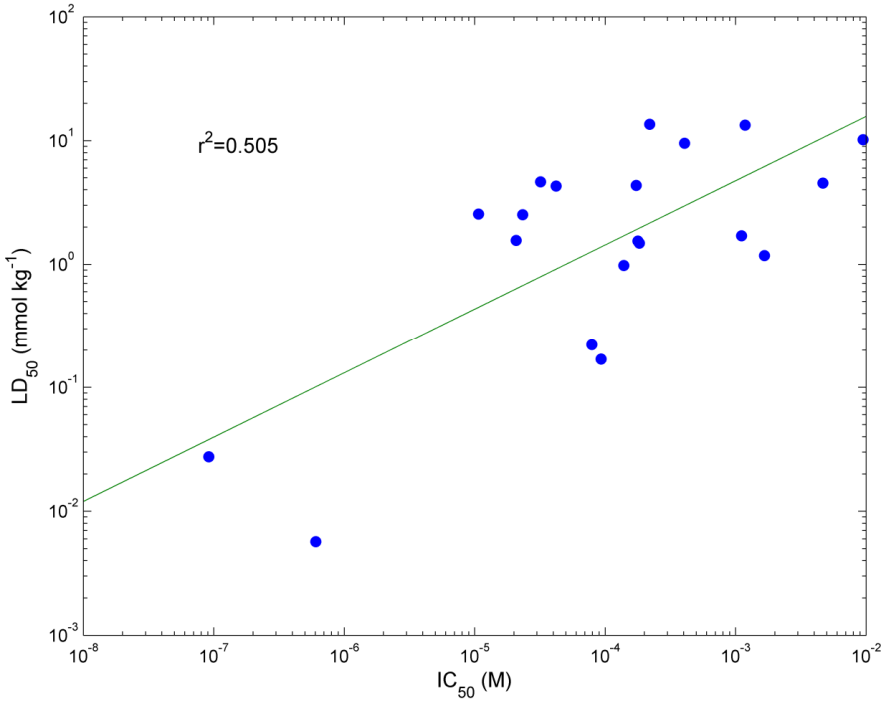

Figure 33. Comparison between IC_{50} and LD_{50} values for the twenty compounds analysed.

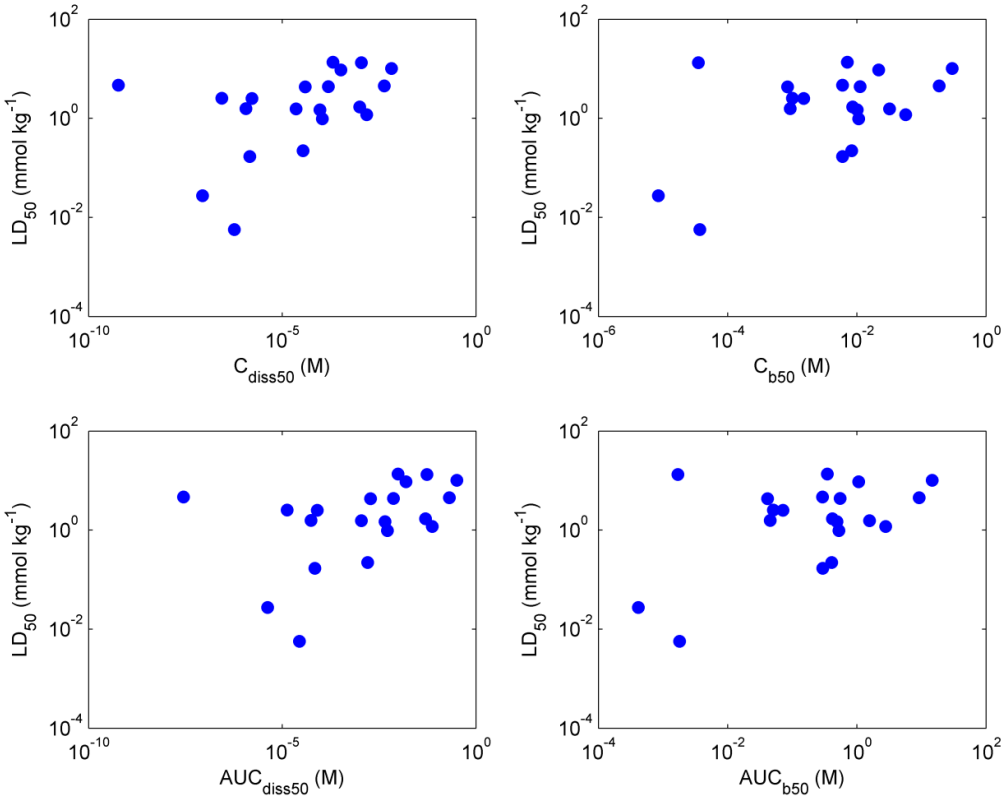

Figure 34. Comparison between the measures in Table 7 and LD_{50} values for the twenty compounds analysed.

3.4. PREDICTION OF 24 h ACUTE TOXICITY IC_{50}s

An application of the model we have tested is the prediction of the concentration-viability response performing the experiments at 24h instead of 48 h. This may be used afterwards as an assessment of the model predictive capabilities. Table 9 shows the results obtained. As it can be observed comparing with Table 3, there is no a clear scaling factor since it changes from chemical to chemical.

Table 9. Estimated 24 h IC_{50} values, using estimated parameters from the 48 h experiments, for the selected chemicals.

Compound	IC_{50} (M) 24 h
Acetaminophen	$4.55 \cdot 10^{-4}$
Verapamil hydrochloride	$8.45 \cdot 10^{-5}$
Acetylsalicylic acid	$9.25 \cdot 10^{-3}$
Maprotiline	$2.52 \cdot 10^{-5}$
Cycloheximide	$8.47 \cdot 10^{-7}$
Sodium lauryl sulfate	$2.10 \cdot 10^{-4}$
tert-Butyl hydroperoxide	$6.01 \cdot 10^{-5}$
Valproic acid	$1.78 \cdot 10^{-2}$
Rifampin	$2.38 \cdot 10^{-4}$
Thioridazine hydrochloride	$1.60 \cdot 10^{-5}$
Amiodarone hydrochloride	$4.41 \cdot 10^{-5}$
Caffeine	$3.94 \cdot 10^{-3}$
Carbamazepine	$7.27 \cdot 10^{-4}$
Colchicine	$2.24 \cdot 10^{-7}$
Acrylamide	$3.03 \cdot 10^{-3}$
Diphenhydramine	$2.90 \cdot 10^{-4}$
Pentachlorophenol	$1.57 \cdot 10^{-4}$
Disopyramide	$2.44 \cdot 10^{-4}$
Chloroquine diphosphate	$3.35 \cdot 10^{-5}$
Tetracycline hydrochloride	$3.68 \cdot 10^{-3}$

3.5. REPEATED DOSE SIMULATION

One of the advantages of developing a model is that it can be used to simulate experiments that are not easy to perform. In this case, once the model parameters have been established, it is possible to try to establish a chronic toxicity value for 3T3 simulating the addition of a constant dose at periodic intervals. This type of assay cannot be carried out *in vitro* easily since medium has to be changed periodically to avoid starvation and cell cultures start to die after a certain period of time. This is similar to the approach followed by Zaldívar and Baraibar (2011) for *Daphnia magna*.

As an example, Fig. 35 shows the simulated results for acrylamide in a 4 days experiment with periodical addition of the same initial dose of the compound each day. As it can be observed, in this case the IC_{50} is around $2.75 \cdot 10^{-4}$ M compared with the value obtained previously in the 48 h experiment which was $1.11 \cdot 10^{-3}$M.

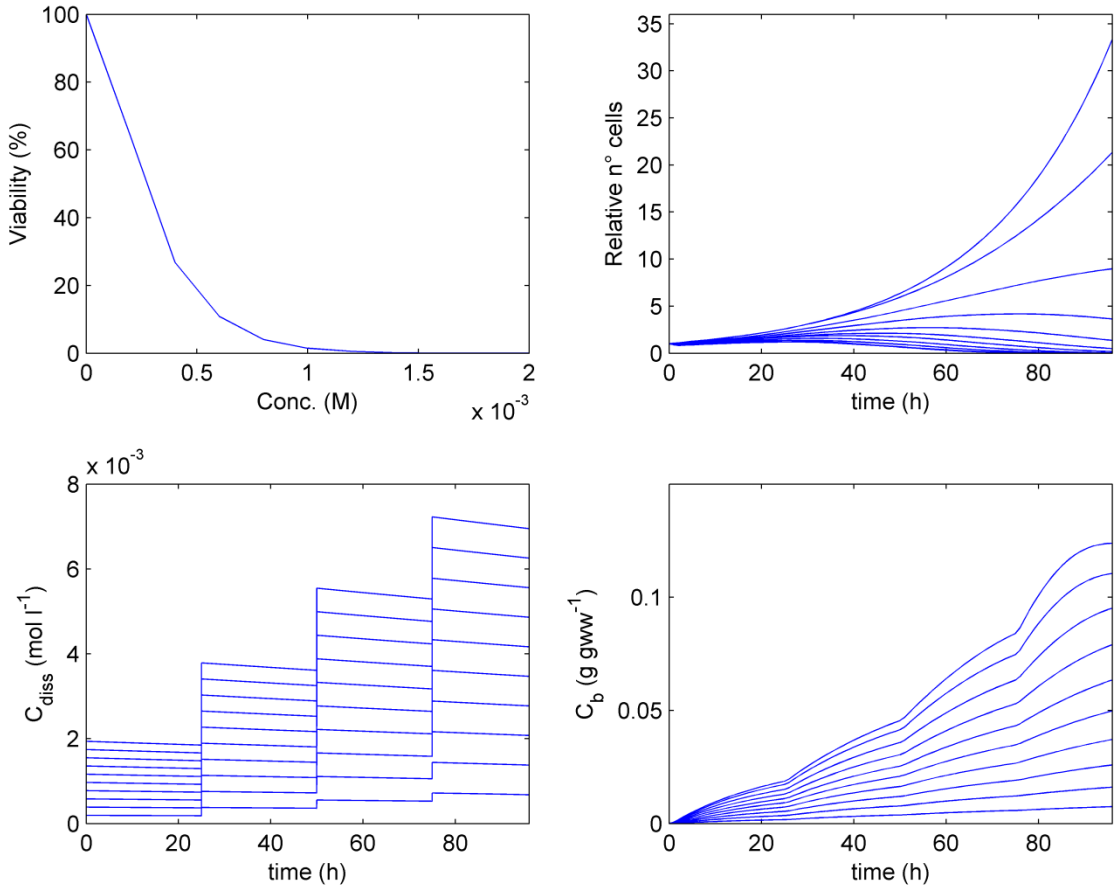

Figure 35. Simulation of repeated dose in-vitro toxicity experiments. Example: Acrylamide with repeated initial dose each 24 h.

4. CONCLUSIONS

A cell growth and toxicity model based on DEB (Dynamic Energy Budget) theory has been developed and implemented to simulate the HTS (High Throughput Screening) laboratory toxicity experiments. The model allows estimating dissolved concentration in the medium as well as internal concentration in the cells.

As the only data available correspond to concentration-response experiments, the validation of the predicted dissolved and internal concentrations has not been possible. The fact that similar fittings can be obtained with different set of parameters can be seen in the second optimization procedure where more parameters were let free. Further research will go in this direction since these values are essential for performing in vitro- in vivo extrapolation. In addition, in parallel we are developing the PBTK models to be able to extract from LD_{50} values the corresponding dissolved and internal concentrations.

Concerning cell population dynamics under increasing concentrations of chemicals, the results obtained correspond qualitatively to the experiments performed using impedance measurements in the Toxcast project (Judson et al., 2011) for the A549 human lung cancer cell line. The next step in the validation of the model will consists on replacing the 3T3 cell growth model by the corresponding

A549 human lung cancer cell line model and then compare for the tested compounds the relative growth curves with the impedance measurements.

Finally a proper sensitivity analysis will be carried out to study the influence of the different parameters on the system dynamics and to assess which factors affect the observed viability variability in the values obtained using replicates in the HTS laboratory experiments. Also the influence of errors in the initial conditions will be assessed. In addition, the differences between the time step of the stage-based model, one hour, probably should be reduced to accommodate fast transient dynamics in the mass balance ordinary differential equations from the medium and the cells.

5. REFERENCES

Beckon, W.N., Parkins, C., Maximovich, A., Beckon, A.V. 2008. A general approach to modelling biphasic relationships. Environ. Sci. Technol. 42, 1308-1314.

Billoir E, Pery ARR, Charles S. 2007. Integrating the lethal and sublethal effects of toxic compounds into the population dynamics of *Daphnia magna*: A combination of the DEBtox and matrix population models. Ecol Model 203, 204-214.

Bouhifd, M. and Whelan, M. 2006. Automated 3T3/NRU standard operating protocol for acute cytotoxicity testing of chemicals. European Commission, JRC, IHCP, InVitech Deliverable No. D2.1.

Bouhifd, M., Casado, J., Coecke, S. *et al.* 2005. Automated process for 3T3/NRU cytotoxicity assay. European Commission, JRC, IHCP.

Bouhifd M, Norlén H, Bories G, Whelan M, Casado Poblador J, Parissis N, Coecke S. Automation and Performance Assessment of a Basal Cytotoxicity Assay Intended for Regulatory Safety Assessment. ADMET Europe 2008 Conference; 19 February 2008; Stockholm (Sweden).

Caswell H. 1989, *Matrix populations models: Construction, analysis and interpretation*, Sinauer, Sunderland, Massachusetts.

Clewell, H. J., Tan, Y. M., Campbell, J. L., and Andersen, M. E. 2008. Quantitative interpretation of human biomonitoring data. *Toxicology and Applied Pharmacology* **231**, 122-33.

Clothier R., Dierickx, P., Lakhanisky, T., Fabre, M., et al. 2008. A database of IC50 values and principal component analysis of results from six basal cytotoxicity assays, for use in the modeling of the in vivo and in vitro data of the EU ACuteTox Project. ATLA 36, 503-519.

Cushing J M. 1998, *An introduction to structured population dynamics*, SIAM, Philadelphia.

DeBruyn, A.M.H. and Gobas, F.A.P.C. 2007. The sorptive capacity of animal protein. *Environ. Toxicol. Chem*. **26**, 1803-1808.

DeJongh, J., Forsby, A., Houston, J.B., Beckman, M., Combes, R., Blaauboer, B.J., 1999. An integrated approach to the prediction of systemic toxicity using computer-based biokinetic models and biological *in vitro* test methods: Overview of a prevalidation study based on the ECITTS Project. Toxicology in Vitro 13, 549-554.

Del Vento, S. and Dachs, J., 2002. Prediction of uptake dynamics of persistent organic pollutants by bacteria and phytoplankton. Environmental Toxicology and Chemistry 21, 2099-2107.

Fuller, E.N., Schettler, P.D. and Giddings, J.C. 1966. A new method for prediction of binary gas phase. diffusion coefficients. Ind. Eng. Chem. 58, 18-27.

Gérard C., Goldbeter A. 2009. Temporal self-organization of the cyclin/CdK network driving the mammalian cell cycle. *Proc Nat. Acad. Sci USA* **106**,21643-21648.

Gubbels-van Hal, W.M.L.G., Blaauboer, B.J., Barentsen, H.M., Hoitink, M.A., Meerts, I.A.T.M. and van der Hoeven, J.C.M. 2005. An alternative approach for the safety evaluation of new and existing chemicals, an exercise in integrated testing. Regulatory Toxicology and Pharmacology 42, 284-295.

Gülden M. and Seibert, H. 2003. *In vitro-in vivo* extrapolation: Estimation of human serum concentrations of chemicals equivalent cytotoxic concentrations *in vitro*. Toxicology 189, 211-222.

Gülden M., Mörchel, S. and Seibert, H. 2001. Factors influencing nominal effective concentrations of chemical compounds *in vitro*: cell concentration. Toxicology *in vitro* 15, 233-243.

Hartwell LH, Weinert TA. 1989. Checkpoints: controls that ensure the order of cell cycle events. *Science* **246**, 629-634.

Heringa, M. B., Schreurs, R.H.M.M., Busser, F., van der Saag, P.T., van der Burg, B., Hermens, J.L.M. 2004. Towards more useful in vitro toxicity data with measured free concentrations. Environ. Sci. Technol. 38, 6263-6270.

ICCVAM, 2006a. In Vitro Cytotoxicity Test Methods for Estimating Acute Oral Systemic Toxicity. Background Review Document. Volumes 1 and 2 (of 2). Interagency Coordinating Committee on the Validation of Alternative Methods (ICCVAM), National Toxicology Program (NTP),

Interagency Center for the Evaluation of Alternative Toxicological Methods (NICEATM), National Institute of Environmental Health Sciences (NIEHS), National Institutes of Health, U.S. Public Health Service, Department of Health and Human Services, November 2006, NIH Publication No. 07-4518.

ICCVAM, 2006b. Test Method Evaluation Report (TMER). In Vitro Cytotoxicity Test Methods for Estimating Starting Doses for Acute Oral Systemic Toxicity. Interagency Coordinating Committee on the Validation of Alternative Methods (ICCVAM), National Toxicology Program (NTP), Interagency Center for the Evaluation of Alternative Toxicological Methods (NICEATM), National Institute of Environmental Health Sciences (NIEHS), National Institutes of Health, U.S. Public Health Service, Department of Health and Human Services, November 2006, NIH Publication No. 07-4519.

Jonker, M.T.O., van der Heijden, S.A. 2007. Bioconcentration factor hydrophobicity cutoff: An artificial phenomenon reconstructed. Environ. Sci. Technol. 41, 7363-7369.

Judson, R.S., Rotroff, D. , Elloumi, F. et al. (2011) . Extracting cellular phenotype kinetic parameters driven by chemical exposure using a real-time cell electronic sensing array (in preparation).

Klanjscek T, Caswell H, Neubert MG, Nisbet RM. 2006. Integrating dynamic energy budgets into matrix population models. Ecol Model 196, 407-420.

Kooijman, S.A.L.M., van Haren, R.J.F., 1990. Animal energy budgets affect the kinetics of xenobiotics. Chemosphere 21, 681-693.

Kooijman SALM, Bedaux JJM. 1996. The analysis of aquatic toxicity data. VU University Press, Amsterdam.

Kooijman SALM. 2000. Dynamic Energy and Mass Budgets in Biological Systems. 2nd Ed. Cambridge University Press, Cambridge, UK.

Kramer, N. I. 2010. Measuring, modelling and increasing the free concentration of test chemicals in cell assays. PhD Thesis. Utrecht University.

Kudryavtsev, A.A., Lavrovskaya,V.P., Popova, I.I.,Lezhnev, E.I., Chailakhyan, L.M., 2004. Estimation of the death rate of 3T3 NIH cell at different phases of the cell cycle in chronic hyperthermia within the physiological temperature range. Doklady Biological Sciences 396, 838-840.

Lopes C; Péry ARR, Chaumot A, Charles S. 2005. Ecotoxicology and population dynamics: using DEBtox models in a Leslie modelling approach. Ecol Model 188, 30-40.

Mackay D. Multimedia Environmental models: The fugacity approach, 2nd Ed., Lewis Publishers: Boca Raton, Florida, 2001.

Meisler, A.I. 1973.Studies on contact inhibition of growth in the mouse fibroblast, 3T3. I. Changes in cell size and composition during 'unrestricted' growth. J. Cell Sci. 12, 847-859.

Migita,S., Funakoshi, K., Tsuya, D., Yamazaki, T., Taniguchi, A., Sugimoto, Y., Hanagata, N., Ikoma, T. 2010. Cell cycle and size sorting of mammalian cells using a microfluidic device. Anal. Methods 2, 657.

Norlén, H., Bouhifd, M., Bories, G., Whelan, M., Casado, J., Parissis, N. Fernando F., Coecke, S. 2007. Report on 3T3/NRU assay results for the testing period January-April 2007. JRC 43733. pp 27.

Pelkonen, O., Coecke, S., Batista Leite, S., Bernauer, U., Bessems, J., Brandon, E., Bois, F., Gundert-Remy, U., Loizou, G., Testai, E. , Zaldívar, J.M. 2011. Toxicokinetics, in Report on alternative (non-animal) methods for cosmetic testing: Current status and future prospects, *Arch. Toxicol.* (in press).

Rotroff DM, Wetmore, BA, Dix DJ, et al. 2010. Incorporating human dosimetry and exposure into high-throughput in vitro toxicity screening. *Toxicological Sciences* **117**, 348-358.

Schotte,W. 1992. Prediction of the molar volume at the normal boiling point. The Chemical Engineering Journal 48, 167-172.

Thomann R.V., 1989. Bioaccumulation model of organic chemical distribution in aquatic food chains. Environ. Sci.Technol. 23, 699–707.

Thomann, R.V., Conolly, J.P., Parkerton, T.F., 1992. An equilibrium model of organic chemical accumulation in aquatic food webs with sediment interaction. Environ. Toxicol. Chem. 11, 615-629.

United States Environmental Protection Agency (US EPA) 1992. Dermal Exposure Assessment: Principles and Applications. EPA/600/8-91/011B. Washington DC. USA.

Van Haren, R.J.F., Schepers, H.E., Kooijman, S.A.L.M., 1994. Dynamic Energy Budgets affect kinetics of xenobiotics in the marine mussel Mytilus edulis. Chemosphere 29, 163-189.

Yazdanian, M., Glynn, SL., Wright, JL., Hawi, A. 1998. Correlating partitioning and Caco-2 cell permeability of structurally diverse small molecular weight compounds. Pharmaceutical Research 15, 1490-1494.

Zaldívar J.M., Mennecozzi M, Marcelino Rodrigues R, Bouhifd M. 2010. A biology-based dynamic approach for the modelling of toxicity in cell-based assays. Part I: Fate modelling. EUR 24374 EN.

Zaldívar, J. M., Campolongo, F., 2000, An application of sensitivity analysis to fish population dynamics, in Saltelli, Chan and Scott (Eds.), Mathematical and Statistical methods for Sensitivity Analysis, Wiley.

Zaldívar, J. M., Baraibar, J., 2011, A biology-based dynamic approach for the reconciliation of acute and chronic toxicity tests: Application to Daphnia magna. Chemosphere (in press)

APPENDIX A. FATE AND TRANSPORT: MASS BALANCE MODEL

This appendix contains the version of the previously developed fate and transport mass balance model (Zaldívar et al., 2010) modified to consider the cells as another independent compartment and not as a part of the medium as it was developed in the previous version.

The fate and transport model consists of a dynamic mass balance that includes a time-variable chemical transport and fate model for calculating the chemical concentration in the medium as well as in the headspace. The gas phase has been included to consider, in a second step, the possible losses and cross contamination between the 96 wells in the TC plates, since the TC are not hermetic even though the system was designed to minimize this aspect. To quantify this phenomenon, there are not enough experimental data at the moment.

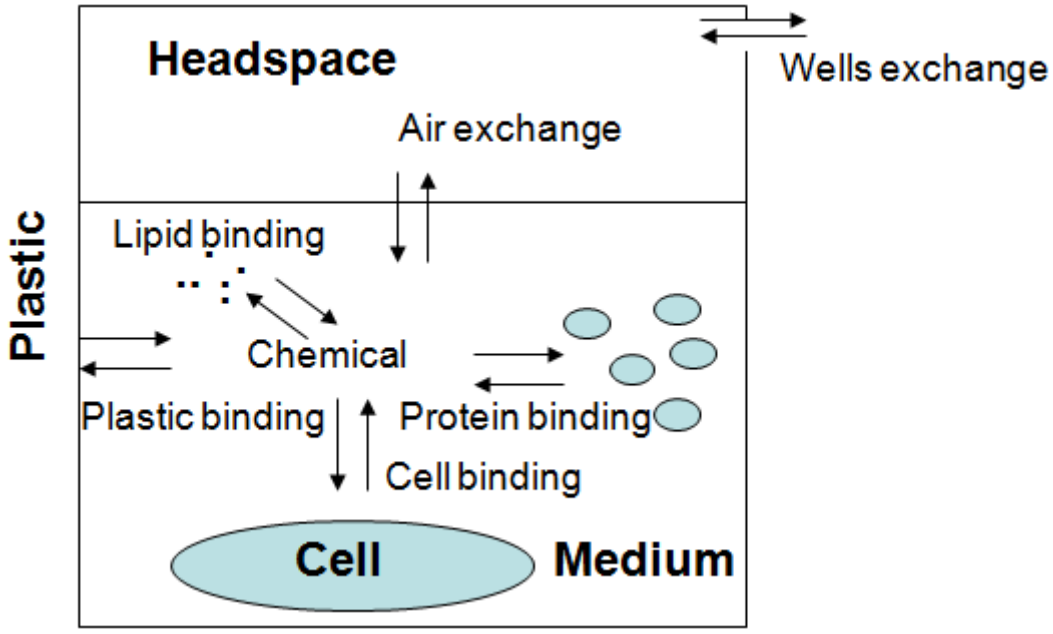

Figure A1. Overview of the process included in the fate and transport model

Assuming a well mixed medium and headspace and that the sorption processes are fast compared with the other processes, then the mass balance equations for both compartments can be written as:

- *Total concentration in the medium*:

$$V_M \frac{dC_T}{dt} = A_s \cdot F_{AW} - R_{upt} - k_{\deg} \cdot V_M \cdot C_{diss} \qquad \text{(A1)}$$

where V_M refers to the volume of the medium (l) and C_T refers to the total concentration (mol l^{-1}); the first term of the rhs represent the transfer of chemical across the air-water interface (A_s), the second term represents the chemical uptake by the cells in (mol s^{-1}) and the third term represent transformation in the medium, e.g. degradation, decomposition, metabolism, etc.

- *Total concentration in the air*:

A similar equation can be written for the headspace:

$$V_H \frac{dC_{air}}{dt} = -A_s \cdot F_{AW} - A_l \cdot F_l - k_{\deg}^{air} \cdot V_H \cdot C_{air} \quad \text{(A2)}$$

where V_H refers to the headspace volume (l); the first term represents the transfer of chemical across the air-water interface, the second term represents the losses from the headspace due to gas exchange, which we will consider zero in this first approach and the third term represent transformation in the headspace, i.e. degradation, decomposition, etc.

To model the partitioning of an organic chemical in the medium (Kramer, 2010), we can consider that the compounds are either purely dissolved (C_{diss}), bound to the serum/proteins (C_S) or to the lipids (C_L) in the culture medium, bound to the (plastic/glass) surface of the culture vessel (C_p) and inside the cells which we model as a different compartment. Therefore, the total concentration of an organic contaminant in the medium, C_T, can be described by following equation:

$$C_T = C_{diss} + C_S + C_L + C_p \frac{S_M}{V_M} \quad \text{(A3)}$$

where S_M refers to the surface of the well in contact with the medium. The partition of the compound between the different phases can be expressed as a function of the total (nominal) concentration in the well as:

$$C_{diss} = \frac{C_T}{1 + K_S \cdot [S] + K_L \cdot [L] + K_p \cdot \frac{S_M}{V_M}} \quad \text{(A4)}$$

$$C_S = \frac{K_S \cdot [S] \cdot C_T}{1 + K_S \cdot [S] + K_L \cdot [L] + K_p \cdot \frac{S_M}{V_M}} \quad \text{(A5)}$$

$$C_L = \frac{K_L \cdot [L] \cdot C_T}{1 + K_S \cdot [S] + K_L \cdot [L] + K_p \cdot \frac{S_M}{V_M}} \quad \text{(A6)}$$

$$C_p = \frac{K_P \cdot C_T}{1 + K_S \cdot [S] + K_L \cdot [L] + K_p \cdot \frac{S_M}{V_M}} \quad \text{(A7)}$$

after defining the following partition coefficients:

-Serum protein partition coefficient K_S ($m^3 \cdot mol^{-1}$) :

$$K_S = \frac{C_S / [S]}{C_{diss}} \quad \text{(A8)}$$

where [S] is the concentration of proteins in the medium (mole protein$\cdot m^{-3}$).

- Lipid partition coefficient, K_L (kg lipid m^{-3})

$$K_L = \frac{C_L / [L]}{C_{diss}} \quad \text{(A9)}$$

where [L] is the concentration of lipids in the medium (kg lipid m^{-3})

- The partitioning constant to plastic, K_p (m):

$$K_p = \frac{C_p}{C_{diss}} \quad \text{(A10)}$$

where C_p (mol m^{-2}) is the concentration sorbed in plastic.

In this approach, we have assumed that the partitioning is fast compared with the rest of the processes.

A. 1. Partitioning of chemicals

A general approach to describe the distribution of the organic compound is by means of the partition coefficients K_i, defined as the relationships between the concentration in a particular medium and in the water. In this case we need to calculate:

- Serum protein partitioning:

Kramer (2010) found the following correlation studying PAHs:

$$\log K_S = 0.37(\pm 0.03) \log K_{ow} - 0.29(\pm 0.12) \quad \text{(A11)}$$

where the partition coefficient K_S is expressed in $m^3 \cdot mol^{-1}$. In a compilation of blood protein (albumin) data DeBruyn and Gobas (2007) for different tissues found that the sorptive capacity of protein in solid animal tissues was higher than K_{ow} for low K_{ow} chemicals ($-1.3 \leq \log K_{ow} \leq 2$) with a value around 1.31(±0.62) (ml g^{-1} albumin). For more lipophobic chemicals ($2 < \log K_{ow} \leq 5.1$) the logarithm of the partition constant increased with log K_{ow} following: 0.57 log K_{ow} +0.69, whereas at higher K_{ow} approached the lipid equivalence value of 0.05, i.e. log K_{ow}-1.3. In addition, they recommended, for modelling purposes, to estimate the sorptive capacity of animal protein as 5% that of lipid.

- Partitioning to lipids:

We have used the same correlation than for lipids inside the cell, i.e. Eq. (28). In this case the amount of lipids in the medium changes from an initial value of 80 10^{-3} kg lipid m^{-3} (Gulden et al., 2001) to a value that depends on the cell mortality since the cell content is supposed to go to the medium.

- Partitioning to well plate plastic:

Kramer (2010) found a linear correlation between K_p and K_{ow} for the PAHs (Polycyclic aromatic hydrocarbons) family.

$$\log K_p = 0.97(\pm 0.15) \log K_{ow} - 6.94(\pm 0.80) \quad \text{(A12)}$$

As an example, if we consider a well with half of the liquid and a hydrophobic compound such as Benzo[a]pyrene (log K_{ow} = 6.13 and log K_p = -0.99), 98% of Benzo[a]pyrene binds to plastic.

A. 2. Air-Water Exchange

Organic pollutants will move in the headspace of the well and since the TC plates are not hermetically close they will diffuse to the other wells during the experiment. The final concentration will depend on the physico-chemical properties of the assessed compound as well as on the dosed concentrations. As a first approximation, we will concentrate on simulating the air-water exchange on a well assuming no transport outside takes place, but we will write the mass balance equation and, when experimental data will become available, we will be able to model the diffusion to other wells in the plate. In this case, the exchange between the headspace and the aqueous medium occurs through diffusive gas exchange between the headspace and medium boundary layer.

- Diffusive exchange

The diffusive air-water exchange flux F_{AW} (mol m^{-2} s^{-1}) at the interface (*i*) is represented as (Westerterp et al., 1984):

$$F_{AW} = k_{AW}\left(\frac{C_{air}}{K_{GL}} - C_{diss}\right) \tag{A13}$$

where C_{air} and C_{diss} are the gas-phase and the dissolved (liquid) concentrations (mol m^{-3}), respectively. K_{GL} is the dimensionless gas-liquid distribution coefficient, $K_{GL} = C_G^i / C_L^i$, and is calculated from the Henry's law constant using:

$$K_{GL} = \frac{H}{R \cdot T} \tag{A14}$$

where R is the universal gas constant 8.314 10^{-3} kJ $(mol \cdot K)^{-1}$ and T is the temperature (K). The temperature dependence of Henry's law constant can be expressed as:

$$\log H = \log H_{298} + \frac{\Delta H_{vap}}{2.303 \cdot R}\left(\frac{1}{298} - \frac{1}{T}\right) \tag{A15}$$

where H_{298} is the Henry's law constant at 25 ºC ($Pa \cdot m^3$ mol^{-1}), ΔH_{vap} is the enthalpy of volatilization from water (kJ mol^{-1}), which have to be defined for each chemical compound.

The mass transfer coefficient k_{AW} (m s^{-1})is given by following equation:

$$k_{AW} = \left(\frac{1}{k_G \cdot K_{GL}} + \frac{1}{k_L}\right)^{-1} \tag{A16}$$

where and k_G and k_L are the mass transfer coefficients (m s^{-1}) in the air and the water films, respectively.

The liquid phase mass transfer coefficient, k_L, is calculated from the mass transfer coefficient of CO_2 in the water side, k_{LCO_2} (Kanwisher, 1963) which when there is no wind has a constant value: $k_{LCO_2} = 4.1 \cdot 10^{-2}$ (m s^{-1}), by applying a correction factor:

$$k_L = k_{LCO_2}\left(\frac{Sc}{600}\right)^{-0.5} \tag{A17}$$

where Sc is the Schmidt number of the pollutant and 600 accounts for the Schmidt number of CO_2 at 298 K. The Schmidt number is defined as:

$$Sc = \frac{\mu}{D_L \cdot \rho} \tag{A18}$$

where ρ and μ are the density and viscosity of the fluid respectively while D_L is the coefficient of molecular diffusion of the dissolved compound. The temperature dependence of the diffusion coefficient in water is calculated with following correlation by Wilke and Chang (1955):

$$D_L = \frac{7.4 \cdot 10^{-12} (\alpha MW)^{0.5}}{\mu \cdot V_b^{0.6}} \cdot T \tag{A19}$$

where T is the temperature of the solvent (K) and μ is its viscosity (cP), V_b (cm^3 mol^{-1}) is the molar volume of the organic compound at its normal boiling point, MW is the molecular weight (g mol^{-1}) of solvent and α is the association factor of the solvent, α = 2.6 for organic solutes diffusing into water (Perry and Chilton, 1984) and D_L is given in m^2 s^{-1}.

The gas phase mass transfer coefficient, k_G, is calculated using the mass transfer coefficient for water, which for the case of no wind has a constant value: $k_{G,H_20} = 3 \cdot 10^{-3}$ (m·s^{-1}), and then

$$k_G = k_{G,H_20}\left(\frac{D_G}{D_{G,H_20}}\right)^{0.67} \tag{A20}$$

where D_G and $D_{G,H2O}$ refers to the diffusion coefficients in the gas phase (air) of the chemical and water, respectively (Schwarzenbach et al., 2003).

An empirical correlation that has been extensively used to estimate the diffusion coefficients in air, D_G in m^2 s^{-1}, as a function of temperature is the one presented in Fuller et al. (1966):

$$D_G = \frac{10^{-7} \cdot T^{1.75}\left(\frac{MW_{Air} + MW_B}{MW_{Air} \cdot MW_B}\right)^{1/2}}{P\left(\left[\sum(\upsilon)_{Air}\right]^{1/3} + \left[\sum(\upsilon)_B\right]^{1/3}\right)^2} \tag{A21}$$

where T is the temperature (K), P is the pressure (atm), MW are the molecular weights (g mol^{-1}) of air (28.8) and the organic compound, and υ are the atomic diffusion values, $\Sigma\upsilon_{Air}$=20.1, that can be determined form the values in Table 1.

Table 1. Atomic diffusion volumes for use in estimating D by the method of Fuller, Schettler and Giddings (1966).

C	16.5	Cl	19.5
H	1.98	S	17.0
O	5.48	Aromatic ring	-20.2
N	5.69	Heterocyclic ring	-20.2

For the specific case of water in air, which is used after to calculate the mass transfer coefficient in the gas phase, we have adjusted the experimental values modifying the atomic diffusion values, i.e. $\Sigma\upsilon_{water}$=10.8., then the diffusion coefficient of water in air is calculated as:

$$D_{G,H_20} = 1.2365 \cdot 10^{-9} T^{1.75} \quad \text{(A22)}$$

A.3. Degradation, Decomposition, Metabolism

In absence of detailed experimental data, degradation, decomposition or metabolism fluxes (mol s^{-1}) are represented as a first order reaction model. Therefore for degradation and decomposition in the medium we will have:

$$F_{\text{deg}}^{M} = k_{\text{deg}} \cdot V_M \cdot C_{diss} \quad \text{(A23)}$$

where C_{diss} is the concentration of the contaminant in dissolved form and k_{degr} may be the degradation rate resulting from hydrolysis, photodegradation, etc. A similar equartion can be written for the headspace:

$$F_{\text{deg}}^{H} = k_{\text{deg}}^{air} \cdot V_H \cdot C_{air} \quad \text{(A24)}$$

Normally, when no detailed data is available, the degradation rate k_{deg} is calculated from half life times

$$k_{\text{deg}} = \frac{\ln 2}{t_{1/2}} \quad \text{(A25)}$$

In this work, we have assessed the effects of considering the use of the half life values provided from the multimedia model installed in EPI Suite v4.0 (see Table 3).

For metabolism, we can assume the same principle and write:

$$F_{met} = k_{met} \cdot C_b \quad \text{(A26)}$$

In this case we have assumed that no metabolism occurs, k_{met}=0, since no data was available for 3T3 cells.

APPENDIX B. NOTATION

$\boldsymbol{A}$	Leslie matrix (describes the transformation of a population from time t, in hours, to time t+1)
A_l	headspace losses surface area (m^2)
A_s	medium-headspace exchange surface area (m^2)
C	Concentrations (mol l^{-1})
C_b	Contaminant concentration in the cell (g gww^{-1})
d_i	duration within i-th stage (h)
D	diffusion coefficient (m^2 s^{-1})
f_x	mass fraction of compartment x (dimensionless)
F	Fecundity rate per unit time (h)
F	molar flow (mol m^{-2} s^{-1})
g_i	growth probability
G_i	Probability of surviving and growing into the next stage $i+1$
H	Henry law constant (Pa m^3 mol^{-1})
k_t	killing rate
K_L	cells-lipids partitioning coefficient (m^3 kg^{-1} lipid)
K_{GL}	gas-liquid distribution coefficient,
K_{ow}	octanol-water partition coefficient
K_P	plastic-medium partitioning coefficient (m)
K_S	partitioning coefficient between serum proteins and medium (m^3 mol^{-1})
k_{AW}	two film mass transfer coefficient (m s^{-1})
k_G	air film mass transfer coefficient (m s^{-1})
k_L	liquid film mass transfer coefficient (m s^{-1})
k	reaction rate constant (s^{-1})
MW	Molecular weight (g mol^{-1})
n	number of moles (mol)
$\boldsymbol{n}_t$	Vector containing number of cells at each stage (G1,S,G2 and M) at time t
NEC	No-Effect Concentration
P	pressure (Pa)
P_i	Probability of surviving and staying in stage i
p	Cell permeability (m)
p_i	Survival probability
R	universal gas constant
r	cell radius (m)
r_{da}	Uptake rate (l $cm^{-2}s^{-1}$)
r_{ad}	Depuration rate (l $cm^{-2}s^{-1}$)
Sc	Schmidt number,
$[S]$	concentration of proteins in medium (mol m^{-3})
S	surface (m^2)
S_M	plastic- medium exchange surface area (m^2)
t	time (s)
T	temperature (K)
V	volume (l)
W	wet weight (g)
z_i	instantaneous mortality rate

Greek symbols

α_G	von Bertalanffy's growth rate
γ_i	Growing probability

ρ	density (g l^{-1})
μ	viscosity (cP)

Subscripts and superscripts

aq	aqueous
AW	air-water
degr	degradation
diss	dissolved
H	Headspace
L	lipids
l	loses
M	medium
p	plastic
P	proteins
S	serum
T	total
w	well

European Commission

EUR 24374 EN – Joint Research Centre – Institute for Health and Consumer Protection
Title: A biology-based dynamic approach for the modelling of toxicity in cell assays: Part II: Models for cell population growth and toxicity
Author(s): José-Manuel Zaldívar, Milena Mennecozzi, Peter Macko, Robim Rodrigues, Mounir Bouhifd and Joaquín Baraibar
Luxembourg: Publications Office of the European Union
2011 – 56 pp. – 21 x 29,7 cm
EUR – Scientific and Technical Research series – ISSN 1831-9424
ISBN 978-92-79-19568-6
doi:10.2788/61603

Abstract. There is a need to extrapolate from *in vitro* concentrations to *in vivo* dose. To do this extrapolation it is necessary to be able to calculate free concentrations in both systems and then compare them. Concerning the in vitro side, in the first part of this work, we had developed and implemented, based on HTS (High Throughput Screening) laboratory data, a compound fate model using the partitioning approach. The developed fate model was able to predict the role of serum in toxicity assays as well as provide estimation on the partitioning of a certain compound between the headspace, plastic wall and the medium: attached to serum, free dissolved and attached to the cells. However, the partitioning approach assumes that the equilibrium is fast in comparison with the duration of the experiments which could not be the case for the partitioning to the cells. For this reason, a DEB (Dynamic Energy Budget) stage-based toxicity model has been developed and experimentally verified in the second part of this work. In addition, the model allows using internal concentrations as the toxicity scale allowing a toxicodynamics' independent raking of the toxic potency of a chemical and the possibility of toxicity data reconciliation from several sources taking into account the inherent dynamics always present during cell-based assays. The results show that this approach opens a new way of analyzing this type of data sets and offers the possibility of extrapolating the values obtained to calculate *in vivo* human toxicology thresholds using a PBPK modelling approach.

How to obtain EU publications

Our priced publications are available from EU Bookshop (http://bookshop.europa.eu), where you can place an order with the sales agent of your choice.

The Publications Office has a worldwide network of sales agents. You can obtain their contact details by sending a fax to (352) 29 29-42758.

The mission of the JRC is to provide customer-driven scientific and technical support for the conception, development, implementation and monitoring of EU policies. As a service of the European Commission, the JRC functions as a reference centre of science and technology for the Union. Close to the policy-making process, it serves the common interest of the Member States, while being independent of special interests, whether private or national.

LB-NB-24374-EN-N